AGU PUBLICATIONS

JGR

Journal of Geophysical Research: Oceans

RESEARCH ARTICLE

10.1002/2016JC011643

Predictability of wind-induced sea surface transport in coastal areas

A. Cucco[1], G. Quattrocchi[1], A. Satta[1], F. Antognarelli[1], F. De Biasio[2], E. Cadau[3], G. Umgiesser[4,5], and S. Zecchetto[2]

[1]National Research Council, Institute for Marine Coastal Environment, Oristano, Italy, [2]National Research Council, Institute for Atmospheric Sciences and Climate, Padova, Italy, [3]Sardegna Clima Onlus, Fonni, Italy, [4]National Research Council, Institute for Marine Sciences, Venezia, Italy, [5]Open Access Center for Marine Research, Klaipeda University, Klaipeda, Lithuania

Key Points:
- Observed and predicted wind data were used as forcings for ocean and particle-tracking models
- Simulation results were compared with a set of observed drifters trajectories
- The predictability of the wind-induced sea surface transport in coastal areas was investigated

Correspondence to:
A. Cucco,
andrea.cucco@cnr.it

Citation:
Cucco, A., G. Quattrocchi, A. Satta, F. Antognarelli, F. De Biasio, E. Cadau, G. Umgiesser, and S. Zecchetto (2016), Predictability of wind-induced sea surface transport in coastal areas, *J. Geophys. Res. Oceans*, *121*, 5847–5871, doi:10.1002/2016JC011643.

Received 13 JAN 2016
Accepted 22 JUN 2016
Accepted article online 27 JUN 2016
Published online 16 AUG 2016

Abstract In this work we investigated the predictability of the wind-induced sea surface transport in coastal areas. The wind fields predicted by two state-of-the-art meteorological models, namely ECMWF and SKIRON, were used as forcing for a hydrodynamic and particle-tracking model applied to reproduce a set of observed drifters trajectories in a coastal area of the Mediterranean Sea. A set of anemometric data derived by in situ measurements were also adopted as model forcing to reproduce the observed drifter paths. This approach provided a baseline that was used as a reference for evaluating the effects of the predicted wind accuracy on the numerical model solution. The accuracy of the simulation results obtained using, as model forcing, the observed wind data was fair and suitable for most of the operational oceanographic purposes. It decreased when using the wind data predicted by the two meteorological models. In particular, the results obtained using ECMWF data were about 3 times more accurate than the ones obtained using SKIRON ones. The uncertainties were strongly dependent on the range of observed wind speed classes with a different behavior depending on the type of adopted wind data. Finally, the amplification of the errors in predicting the sea surface transport generated by the inaccuracies of the predicted wind fields was quantified.

1. Introduction

The Lagrangian transport or material transport is the transfer of quantities along the motion of some carrying fluid. This process is of fundamental importance for many different branches of the geophysical fluid dynamic [*Ottimo*, 1989; *Samelson and Wiggins*, 2006; *Lin*, 2013]. In oceanography, the Lagrangian transport refers to the advection of quantities dispersed or dissolved in the water column due to the combined action of marine currents, winds, and waves. Its estimate plays a fundamental role in many applications including search and rescue missions (SAR), management of oil spills emergencies, accident localization via backward tracking of the floating debris, estimate of larval, and sediment transport for fishery and coastal management. These are just some of the activities for which establishing the origin or the fate of a given water mass is essential to enhance the understanding of the investigated processes [*Döös et al*., 2011].

The transport at the sea surface can be measured by Lagrangian current meters, generally known as drifters, which are floating and water following instruments that provide direct and localized information of the surface transport [*Davis*, 1985]. As an example, in many SAR missions, drifters are deployed at the last known position with the hope of identifying the ocean currents in the region at the incident time [*Brushett et al*., 2016].

While the measurement of the sea surface transport is carried out using drifters [*Poulain*, 2001], its forecasting is performed following a numerical approach commonly based on the use of coupled ocean and particle-tracking models. Although the process is very complex, since the motion of particles advected by the ocean currents is typically chaotic [*Griffa et al*., 2004], in recent years considerable improvements have been achieved to numerically reproduce it [*Özgökmen et al*., 2001; *van Sebille et al*., 2009; *Lumpkin and Elipot*, 2010; *Huntley et al*., 2011].

The increase of the models resolutions, the availability of data assimilation techniques as well as the use of specific dynamical system methods to compute the Lagrangian transport greatly improved the accuracy of the numerical predictions [*Olascoaga et al*., 2006]. In fact, trajectory models have proved appropriate for

© 2016. American Geophysical Union. All Rights Reserved.

analyzing the ocean circulation [*Blanke et al*., 2001; *Speich et al*., 2002; *Drijfhout et al*., 2003; *Döös et al*., 2008] and as a support to maritime and pollution accidents [*Foreman et al*., 2005; *Sayol et al*., 2014] and they also have been useful in the biological context [*d'Ovidio et al*., 2009; *Cermeño and Falkowski*, 2009; *Serra et al*., 2010].

Many authors tested the models accuracy by means of a direct comparison between observed and predicted trajectories [*Johnson and Pattiaratchi*, 2004; *Caballero et al*., 2008; *Beg Paklar et al*., 2008; *Spydell et al*., 2015]. Specific sensitivity analyses were carried out to define the role of the numerical model parameterizations on changes in the accuracy of the sea surface transport prediction. The importance of a correct reproduction of the surface velocity shear as well as of the wind drag and Stokes drift contribution to the total transport was also analyzed [*Furnans et al*., 2008; *Edwards et al*., 2006; *Carniel et al*., 2009].

In coastal areas, if astronomical tides are weak and no intense estuarine processes occur, the wind is often the main forcing the surface water circulation. This is the case of many coastal areas of marginal seas at the midlatitudes as the subbasins of the Mediterranean Sea [*Cucco et al*., 2006].

The wind and the other meteorological quantities (e.g., thermal fluxes and air temperature) used to perform oceanographic predictions are generally provided by atmospheric numerical models operating within operational weather prediction systems.

The role of these forcings in simulating the oceanographic processes has been widely investigated mainly for open oceans and for specific variables such as sea surface temperature, wind waves height, and sea level [*Cavaleri and Bertotti*, 1997; *Manca et al*., 2002; *Zavatarelli*, 2002; *Wakelin and Proctor*, 2002; *Signell et al*., 2005; *Brenner et al*., 2007].

Only recently, few studies evaluated the effects of the uncertainties in the predicted wind fields on the accuracy of the sea surface transport forecasting [*Beg Paklar et al*., 2008; *Lebeaupin Brossier et al*., 2011; *Brushett et al*., 2011; *Lebeaupin Brossier et al*., 2012]. In all these studies, the accuracy of the numerical predictions was determined by comparing the simulations results obtained using, as model forcing, different predicted wind data sets, with observed drifter trajectories. Under no circumstances, the sea surface transport was previously reproduced using observed wind data as model forcing. Such an approach would allow to define a baseline to be used as a reference when evaluating the effects of the accuracy of the predicted winds on the numerical model solution.

In this work we investigated the predictability of the wind-induced sea surface transport in a coastal area of the Mediterranean Sea, namely the Gulf of Oristano (see Figure 1). An ocean and particle-tracking model was implemented and used to reproduce the wind-induced water circulation and the sea surface transport in the area. The adopted numerical tool consisted in a three-dimensional hydrodynamic and a particle-tracking model based on the finite elements method particularly suitable for shallow water environments (SHYFEM) [see *Umgiesser et al*., 2004].

The wind data predicted by two different weather prediction systems were tested as model forcing. More precisely, two state-of-the-art atmospheric numerical models were employed: the atmospheric prediction system of the European Centre for Medium Weather Forecast (ECMWF) based on a global hydrostatic numerical model and the SKIRON prediction system [*Kallos*, 1997; *Papadopoulos et al*., 2001], based on regional nonhydrostatic model.

The surface transport was measured during two field campaigns by deploying Lagrangian drifters in the Gulf under moderate and intense wind conditions. In the survey area a specifically implemented wind measuring system provided surface wind speeds and directions derived by in situ measurements. These data were used as model forcing and the obtained results compared with observed drifters trajectories in order to define a baseline to be used as a reference when evaluating the predictability of the sea surface transport. This reference was used to quantify the uncertainties in the numerical prediction arose when using, as model forcing, the wind data sets produced by the two weather prediction systems.

The paper is organized as follows: a brief description of the Oristano Gulf including the morphological and oceanographic features is reported in section 2; the wind measuring system and the two weather prediction systems are described in section 3; the experimental and the numerical approaches followed to measure and to predict the surface transport are illustrated in section 4; in section 5, the observed Lagrangian

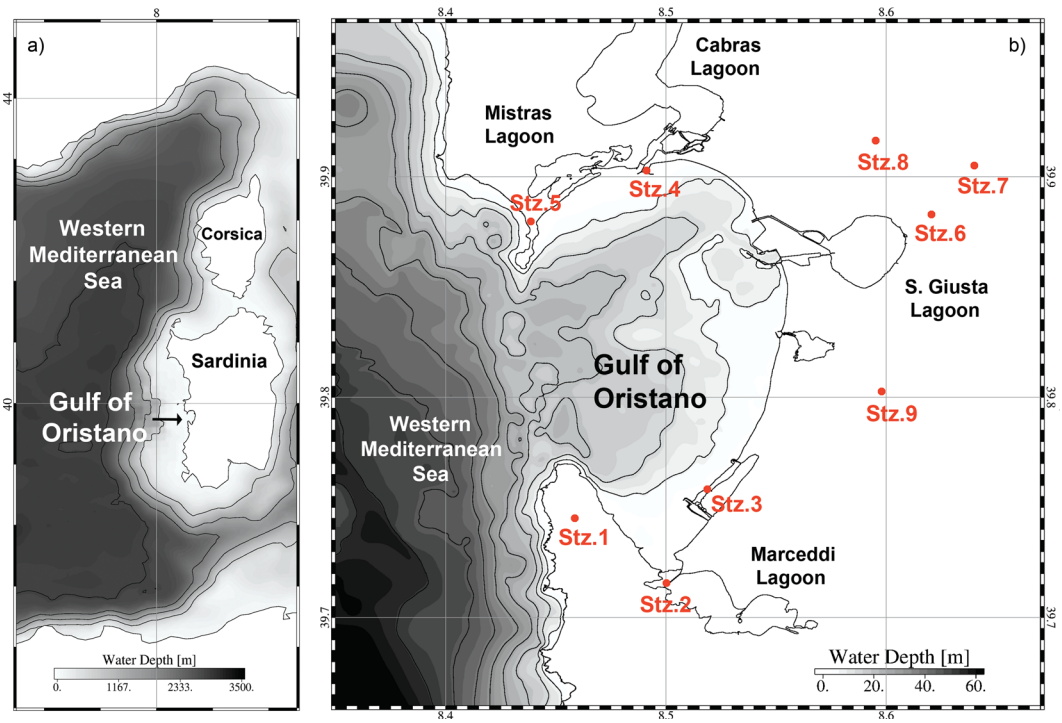

Figure 1. Geographical setting: (a) location of the Oristano Gulf in the Western Mediterranean Sea and (b) geographical and bathymetric features of the Gulf. Red dots indicate the position of the anemometric stations (Stz. 1–9).

velocities and trajectories are compared with the ones computed using the observed and the predicted wind fields as model forcing; finally, the errors in predicting the sea surface transport using different meteorological data set are quantified and discussed.

2. Site Description

The site selection was driven by the objective of minimizing the contribution to the sea surface transport of the other meteo-marine forcings except the wind, such as the tides, the thermohaline forcings, and the wind waves action. The Gulf of Oristano (see Figures 1a and 1b), located along the West Sardinian coastline, in the Western Mediterranean Sea, approximately between 8.4°E and 8.6°E and 39.7°N and 39.9°N, was evaluated as particularly suitable for this purpose. It is a semienclosed basin connected to the Sardinian Sea by a 9 km wide opening between two rocky capes. It covers a surface of approximately 50 km^2 with maximum water depth of about 25 m and an average value of about 12 m.

The offshore circulation is mainly characterized both by low-energetic anticyclonic gyres generated by the baroclinic instabilities of the Algerian current system and by the absence of intense thermohaline currents along the continental margin [*Millot*, 1999; *Olita et al*., 2013]. A wide and relative shallow area characterized by water depths ranging between 30 and 150 m extends up to 15 km offshore the Gulf strongly reducing the possible influence of the open sea circulation on the bay hydrodynamics [*Cucco et al*., 2006].

The freshwater sources, with an yearly average lower than 5 $m^3\ s^{-1}$, are characterized by torrent like regimes and do not contribute to the generation of any horizontal density gradients able to influence the Gulf hydrodynamics [*Cucco et al*., 2006].

The tidal forcing is negligible, being the amplitudes very weak, around 0.15 m [*Ferrarin and Umgiesser*, 2005; *Cucco et al*., 2012a; *Umgiesser et al*., 2014], and not producing any remarkable pressure gradient along the basin [*Cucco et al*., 2006].

The wind waves, mainly from north-west and south-west, are sheltered by the presence of the two capes, with the consequence that most of the basin is not exposed to the direct wave action [*De Falco et al*., 2008].

Furthermore, the wind waves from north-west, the most frequent and energetic, are partially dampened in the relative shallow water areas (around 25 m depth) extending offshore the Gulf and by the presence of the Mal di Ventre island with an extended shallow bank located 15 km offshore and north-west of the Gulf [*Simeone et al*., 2014].

The wind climate is characterized by three main regimes: wind from north-west (Mistral wind), from south-east (Sirocco wind), and from south-west (Libeccio wind). The Mistral wind is the most frequent (∼45%) and strong, followed by Libeccio (∼15%) and Sirocco (∼25%). The yearly mean speeds vary between 7 m/s for Mistral, 5 m/s for Sirocco, and 6 m/s for Libeccio regime [*Ferrarin and Umgiesser*, 2005].

Most of the time, the water circulation inside the Gulf and the induced surface transport are promoted by the direct action of the wind. In particular, due to the absence of strong bathymetric gradients and to the relative large mouth of the bay, any remarkable tilting of the sea surface generated by the wind action and able to promote the seiches phenomenon was not found [*Cucco et al*., 2006].

3. Wind Measurements and Predictions

Assuming the wind is the main meteo-marine forcing the water circulation in this coastal area, the numerical prediction of the sea surface transport is strongly dependent on the predictability of the adopted wind fields.

With the aim of evaluating this dependency, we considered a Wind Measuring System (WMS, hereafter) providing direct measurements of the wind speeds and directions for the Oristano Gulf area and two different Weather Prediction Systems (WPS, hereafter), based on different meteorological models, both delivering short-term predictions of the main meteorological parameters, including the wind. In the following, the description of the three systems is reported.

3.1. The Wind Measuring System

The WMS of the Oristano Gulf has been developed under the framework of the Italian flagship project RITMARE (http://www.ritmare.it) and consists of five three-components anemometers located along the Gulf coastline (see Figure 1, Stz. 1–5) and of four standard cup anemometers located inland (few km from the coast, sites 6–9). The inland instruments are part of the weather network of Sardegna Clima Onlus (http://www.sardegna-clima.it). All the anemometer propellers were calibrated before installation. The acquisition process is continuous at a sampling rate of 1 Hz. The inland stations provide the wind speed and direction as well as the air temperature and the atmospheric pressure.

The anemometers are located at different altitude, varying between 2 and 93 m above the sea level. The conversion of the measured wind speed to the wind speed at 10 m was performed using a boundary layer model derived from the boundary layer theory [*Monin and Obukhov*, 1954]. This requires, besides the wind speed, the stability conditions essentially expressed by the air-sea temperature difference. The air temperature was provided by the WMS, whereas the sea surface temperature was obtained from satellite data furnished by the Operational Sea surface Temperature and sea Ice Analysis system (OSTIA) [see *Stark et al*., 2007].

Ad hoc interpolation procedure based on two-dimensional method developed by *Brocchini et al*. [1995], already tested for similar application in the Venice Lagoon [*Zecchetto et al*., 1997], was used to regrid the scattered wind data (red dots and vectors in Figure 2a) over a regular mesh with 0.01° grid size covering the whole Oristano Gulf (black vectors in Figure 2a). This specific interpolation method, suited to grid spatially sparse observations, and the configuration of the anemometer positions almost surrounding the Gulf allowed to realistically estimate the wind fields in the area.

The WMS data were already used with success in previous studies as, for instance, in *Zecchetto et al*. [2016], where the wind fields produced by the WMS were compared with the wind fields extracted from Synthetic Aperture Radar satellite images in the Gulf. The two data sets were compatible in terms of both temporal and spatial variance confirming the WMS data as realistic proxy of the surface winds in the basin. We refer to this study for a detailed evaluation of the WMS data.

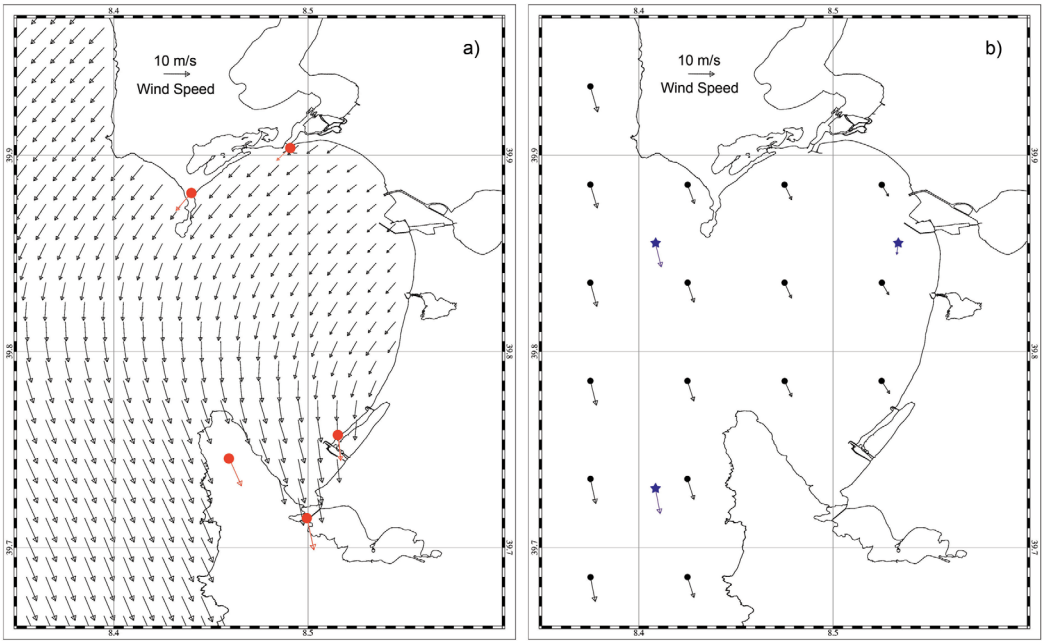

Figure 2. The 10 m wind field in the Oristano Gulf: (a) as estimated by the WMS, red dots and vectors refer to the anemometers positions and measured wind; (b) as predicted by ECMWF, blue stars and vectors refer to the mesh nodes and predicted wind vectors, and as predicted by SKIRON, black dots and vectors. All data refer to the 06:00 A.M. of 24 July 2014.

The WMS operates since January 2014 delivering, in real time through a Web interface, hourly maps of wind fields over the Gulf and surroundings. A detailed description of the system and adopted methodology can be found in *Zecchetto et al.* [2016, 2016a].

3.2. Weather Prediction Systems

Two different types of WPS and predicted wind fields were considered: the one developed and maintained at the European Centre for Medium-range Weather Forecasts (ECMWF) in Reading, UK, and the one developed and maintained at the National and Kapodistrian University of Athens, GR, known as SKIRON forecasting system [*Kallos*, 1997]. The two WPS differ for several aspects including the type of numerical model, the model spatial resolution, and the covered domain.

ECMWF uses a global atmospheric model (T1279 model version) based on the hydrostatic approximation with a horizontal spatial resolution of 0.125° and 137 levels for the vertical discretization. Wind fields at 10 m as well as several other atmospheric variables are predicted daily within a forecasting time lag of 10 days and variable time steps (1, 3, and 6 h). The ECMWF is established to be the reference WPS in the Meteorological Scientific Community at European level [*Lynch*, 2008] and their predicted data set are widely used as input data for most of the European oceanographic prediction systems.

SKIRON is based on a dynamical downscaling [*Giorgi*, 2006] of the ETA/National Center for Environmental Prediction (NCEP) model initially developed by *Janjić* [1984]. It is a nonhydrostatic model applied to a domain covering the whole Mediterranean Sea and part of the North Atlantic basin [*Kallos and Pytharoulis*, 2005]. The mesh horizontal spatial resolution is 0.05° and the vertical domain is discretized by 45 vertical levels stretching from surface to 20 km. Initial and lateral boundary conditions are provided by NCEP/GFS (http://www.nco.ncep.noaa.gov/pmb/products/gfs). Wind fields at 10 m and other meteorological variables are predicted daily with hourly frequency and within a forecast interval of 5 days. The SKIRON meteorological products are widely used in Mediterranean countries for different purposes spanning from oceanography to meteorology [*Koçak et al.*, 2012; *Agüera-Pérez et al.*, 2012; *Alves et al.*, 2015].

As an example, in Figure 2b, the ECMWF and SKIRON mesh nodes and predicted wind vectors are reported with different colors for the Oristano Gulf sea surface area for the 24 July 2014, 06:00 GMT.

4. Sea Surface Transport: Measurements and Predictions

Numerical modeling techniques, based on coupled hydrodynamic and particle-tracking models, are widely used to reproduce and predict the sea surface transport due to the combined action of surface currents and wind forcing.

The high-resolution ocean and particle-tracking model SHYFEM [*Umgiesser et al.*, 2004] was implemented to simulate the basin water circulation and the sea surface transport promoted by the wind only. Two field campaigns were carried out to measure the effective transport by releasing a set of drifters when moderate and intense winds were forcing the basin water circulation. These Lagrangian measurements were performed during July 2014 and January 2015, under a set of different wind conditions representative of the local anemometric climate.

In the following, the drifters data collected during the field campaigns as well as the numerical approach followed to predict the sea surface transport are described.

4.1. The Lagrangian Measurements

The GPS-equipped mini drifters MD03 (http://albatrosmt.com/mini-drifter-buoy-md03) based on the Global System for Mobile communication (GSM) were used. Each drifter was equipped with a temperature sensor and a plastic drogue for a total weight of 2 kg and a length of 45 cm with the neutral buoyancy level located at around 8 cm from the top. Drifter positions and water temperatures were recorded at 5 min intervals and communications occurred each 30 min via Short Message System (SMS). The adopted configuration was particularly suited for short-term experiments aimed to measure the surface circulation in coastal waters [*Quattrocchi et al.*, 2016]. A total of 16 drifters were released in the Gulf during an overall period of 20 days, 7 days in summer, between 23 and 30 July 2014, and 13 days in winter, between 17 and 30 January 2015.

In Figure 3, the paths followed by the whole set of drifters are reported for both experiments. Most of the trajectories were confined in the northern and central part of the Gulf with a spatial coverage including

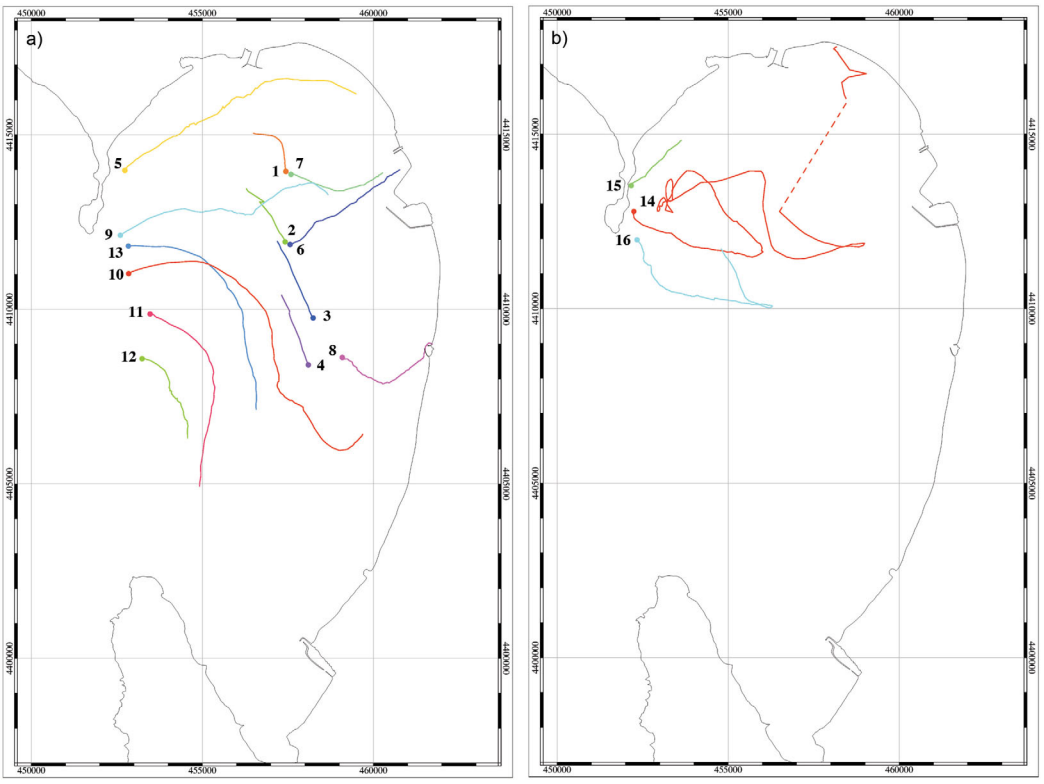

Figure 3. The paths followed by the drifters released in the Gulf during the two experiment: (a) summer period and (b) winter period. Colored dots indicate drifters initial positions. Dashed line indicates missed data due to GSM communication problems. The geographical reference system is expressed in meters following Gauss projection in order to facilitate the comparison between speed and distance units.

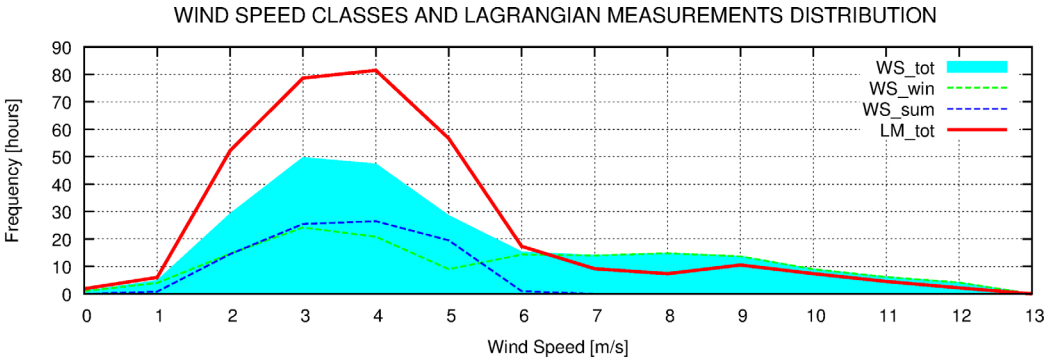

Figure 4. Frequency of observed wind speed classes during the two experiments (WS_tot), during the summer experiment only (WS_sum) and during the winter experiment only (WS_win). LM_tot indicates the duration of the Lagrangian measurements in relation to each observed wind speed class.

both the shallow and the deep parts of the basin. The average ratio between each path length and the total displacement from the initial position was 0.71 indicating, for most of trajectories, a quasi-linear path. Trajectories lengths varied between 1.1 and 26.6 km with average length of 5.1 km. The observed maximum displacement from the initial release was 10.1 km and the average value for the whole set was 3.2 km.

In Figure 4, the distribution of the measurements duration (LM_tot) is reported as a function of the wind speed measured by the WMS. A total amount of 336 h of Lagrangian observations were obtained, characterized by a minimum and a maximum time interval spent in water for the whole set of drifters, of about 4 and 78 h, respectively.

During the two investigated periods, the winds were representative of the local anemometric climate [*Ferrarin and Umgiesser*, 2005], with speeds varying between 1 and 13 m/s (see WS_tot in Figure 4) and directions varying between northwest, southeast, and southwest. In particular, in the summer experiment the wind directions varied between the southeast, southwest, and northwest, corresponding to Sirocco, Libeccio, and Mistral regimes, with speeds ranging between 1 and 7 m/s (see WS_sum in Figure 4) whereas during the winter experiment, the wind was mainly from northwest, corresponding to Mistral regime, with observed speeds up to 13 m/s (see WS_win in Figure 4).

The surface water temperatures measured by the drifters varied between 24 and 26°C during the summer experiment and between 13 and 15°C during the winter period. The maximum spatial variations were measured in summer period with maximum differences in temperatures of 0.7°C and with an average variations of 0.4°C computed along a distance of about 5 km. In winter the spatial variation was lower, around 0.1°C computed for similar distances.

4.2. The Numerical Prediction

The three-dimensional finite element hydrodynamic model, SHYFEM [*Umgiesser et al.*, 2004], was adopted to reproduce the Oristano Gulf wind-induced water circulation. The model, already used with success, for reproducing the main hydrodynamics in the Gulf and surrounding lagoons system [*Ferrarin and Umgiesser*, 2005; *Cucco et al.*, 2006; *Magni et al.*, 2008; *Cucco et al.*, 2012a; *Coppa et al.*, 2013; *Umgiesser et al.*, 2014; *Ferrarin et al.*, 2014; *Quattrocchi et al.*, 2016] resolves the shallow water equations integrated over each layer in their formulations with water levels and transports.

The simulation of the drifter trajectories was carried out using a particle-tracking module coupled off-line with the hydrodynamic model, which computes the sea surface transport due to the marine currents and wind contribution [*Cucco et al.*, 2009, 2012b; *Melaku Canu et al.*, 2015; *Cucco and Umgiesser*, 2015].

A description of the solved equations system is reported in Appendix A whereas the adopted numerical treatment is reported in *Umgiesser et al.* [2004].

4.2.1. Model Setup

The model domain was selected between 7.8°E and 8.6°E and between 39.2°N and 40.5°N, including the Gulf of Oristano, the surrounding coastal areas and part of the western Mediterranean Sea (see Figures 5a and 5b).

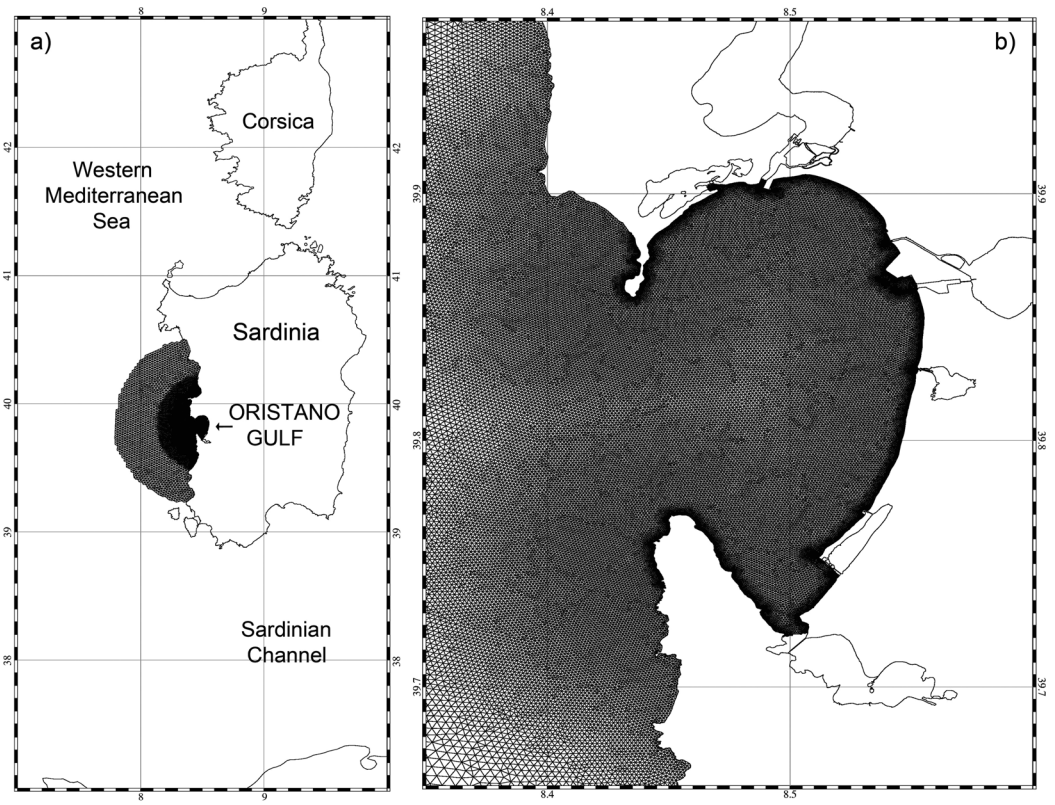

Figure 5. Finite element mesh adopted for the numerical simulations: (a) the total domain and (b) the zoom for the Oristano Gulf.

A finite element mesh composed of 45,065 nodes and 88,229 triangular elements with a spatial resolution varying between around 20 m for the Gulf coastal areas and few km for the far field was used for the horizontal discretization (see Figures 5a and 5b). The vertical direction was defined by 45 z-levels with layer depths ranging between 0.5 and 200 m following an ad hoc step distribution.

The reduced extent of the interest area, its confinement in relation to the overall mesh width, and the assumptions made allowed us to set the whole model borders as closed boundaries with full slip conditions.

A scale analysis was carried out to evaluate the weights of the main forcing terms in the momentum equation for the specific numerical experiments (see Appendix B). The obtained results suggested that the baroclinic pressure gradients could be neglected.

Regarding the tides, in *Quattrocchi et al*. [2016], a similar numerical experiment was performed to reproduce the surface transport in a lagoon connected to the Oristano Gulf, and the results revealed that the tide was not producing any remarkable contribution to the local hydrodynamic compared to the one produced by the wind action.

The density vertical distribution was set as homogeneous and the GOTM turbulence closure model [*Burchard and Petersen*, 1999] was used to reproduce the momentum transfer between the layers without any constrain related to the buoyancy variability along the vertical. The use of un-stratified model setup is generally acceptable in the case the domain of interest is not affected by estuarine processes [*Spydell et al*., 2015]. Furthermore, the basin water depth was shallow enough and the wind speeds during the two investigated periods were strong enough to consider the water column as homogeneous.

Therefore, the wind was set as the only external forcing promoting the Gulf water circulation. In particular, only a restricted part of the model domain, corresponding to the area covered by the WMS interpolation grid (see Figure 2a) was subjected to the wind drag action.

The particles-tracking model, implemented on the same unstructured mesh, used, as input data, the current fields computed at 0.5 m and the hourly data of measured or predicted wind fields. The wind wave Stokes

drift contribution to the surface transport was neglected being the Gulf mostly sheltered by intense wind waves.

The hydrodynamic model time stepping was subjected to Courant criterion and set to be variable in time, whereas a 300 s constant time step was selected for the particle-tracking model, being it not subjected to time step constraining [*Cucco et al*., 2009].

4.2.2. Simulations Setup and Lagrangian Metrics

The model was run to simulate the drifters trajectories using, as forcing, the three different types of wind fields previously described: those derived from the WMS data and the ones predicted by ECMWF and SKIRON.

For each type of wind forcing, two different simulations were carried out to reproduce the water circulation and the drifters trajectories inside the Gulf during the two measuring periods. The duration of each simulation run was about 30 days including a spin-up time of 10 days, established to be enough to damp out the noises due to the imposed initial conditions, set as a no motion state. The obtained current fields computed at 0.5 m depth along with the wind fields data were used as input for the particle-tracking module to reproduce the 16 drifters trajectories.

In the reference scenario (WMS scenario, hereafter), the hourly fields of wind speeds and directions derived by the WMS anemometric data were used as model forcing. For the other two scenarios (ECMWF and SKIRON scenario, hereafter), the wind data were obtained by concatenating the first 24 h forecast fields of each daily ECMWF/SKIRON run, so to keep the forecast time lag always between 1 and 24 h.

A linear interpolation was used to compute, at each simulation time step, the wind speed components at the nodes of the SHYFEM model mesh (see Figure 5) starting from the hourly data estimated and predicted at the WMS and WPS grids points (see Figure 2).

For each simulation run, at each observed drifter position, 225 numerical particles were released and their trajectories computed. The number of released particles was established on the basis of a statistical procedure [*Cucco et al*., 2012b]. For each scenario, a total of 907,200 numerical trajectories were computed.

As an example, in Figures 6a and 6b, the observed trajectories along with the paths obtained from the WMS scenario are reported for two selected drifters experiments (the 5th and the 14th of Figure 3). Red lines represent the observed trajectories, green lines the average trajectories computed for each group of particles released at each observed drifter position, and, finally, the black lines the average trajectories computed for the first group of particles released at the drifters starting positions.

The accuracy of the simulations results was estimated throughout the comparison between the observed and the computed horizontal components of the Lagrangian current velocities. A total of 328 observed velocities were obtained from the whole set of observed drifters trajectories. The observed velocities were

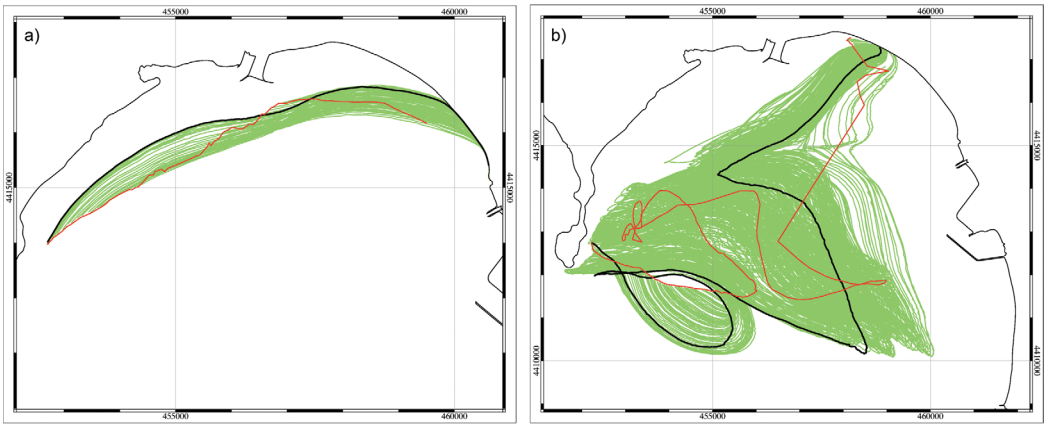

Figure 6. Observed and simulated trajectories for two different drifters releases: (a) the 5th and (b) the 14th of Figure 3. Red lines represent the observed trajectories, green lines represent the average trajectories computed for each group of released particles and gray lines represent the average trajectories followed by the groups of particles released at the drifters starting positions.

computed at hourly frequency and for each drifter trajectory, as the distance covered by each drifter divided by the time.

Furthermore, a degree of predictability of the computed trajectories as a function of the forecasting time lag was defined. From simulations results, at hourly frequency, the distances between the average position of each group of numerical particles and the corresponding drifter location were estimated obtaining the Trajectory Absolute Error (TAE), which is defined as

$$\mathrm{TAE}(t)=\left\langle \sqrt{(x_d-x_m)^2+(y_d-y_m)^2}\right\rangle_{nd}, \tag{1}$$

with x and y corresponding to the components of the drifter positions at the time t and the subscript d and m indicating observations and numerical particles, respectively. The average was performed for the whole set of released particles nd. Then, the ratios between the computed TAE and the corresponding drifters paths lengths were calculated obtaining the Trajectory Relative Error (TRE), defined as

$$\mathrm{TRE}(t)=\frac{\mathrm{TAE}(t)}{\sum_{i=2}^{p}\sqrt{(X_i-X_{i-1})^2+(Y_i-Y_{i-1})^2}}, \tag{2}$$

with X and Y the components of the drifter positions along the trajectory and p indicating the last position at time t. Under different acronyms, both TAE and TRE are found in literature as common functions to estimate the performances of particle-tracking models [*Griffa et al*., 2004; *Yaremchuk et al*., 2013; *Berta et al*., 2014; *Brushett et al*., 2016].

TAE is expressed in meters, whereas TRE is a positive and nondimensional number. In particular, TRE = 0 corresponds to a perfect match between the observed and the computed trajectories, TRE = 1 corresponds to a difference between the predicted drifter position and the observed one equal to the total observed path length.

The TRE and TAE values were grouped on hourly basis considering a prediction time lag ranging between 1 and 24 h from the release, obtaining the evolution of the model accuracy as a function of the forecast time lag.

5. Results and Discussion

In Figure 7, the observed and computed trajectories are reported for the whole set of experiments and for all the three scenarios. For the sake of clarity, only the average paths obtained by the groups of particles released at each drifter initial position are reported.

In the WMS scenario, for most of the experiments, the computed trajectories (gray lines in Figure 7) reproduced satisfactorily the drifter paths (red lines in Figure 7). Qualitatively, all the computed paths followed the same directions of the measurements without any noticeable divergence from the observed trajectories. On the contrary, the paths obtained from ECMWF and SKIRON scenarios (black and blue lines in Figure 7) were not always in agreement with measurements.

For each scenario, the accuracy of the simulations results was evaluated by both comparing the observed and the computed Lagrangian velocities and by estimating the TRE and the TAE.

The results obtained from the WMS scenario were considered as the reference and compared with those from the other scenarios to estimate the influence of the predicted wind data sets on the model accuracy.

5.1. Observed and Computed Sea Surface Currents

In Table 1, the average and maximum values of the observed and computed Lagrangian current velocities are reported. The current speeds observed during the two experiments were on average 0.11 m/s with a peak value of 0.53 m/s measured during the winter period (see AVG_t and MAX_w in Table 1).

In the WMS scenario, the average current speed was similar to the observed one with a value of 0.09 m/s. In the ECMWF scenario, the average predicted current speed was also similar to the observations with a value of 0.08 m/s, whereas when using SKIRON wind data as model forcing, the computed value was lower, around 0.05 m/s.

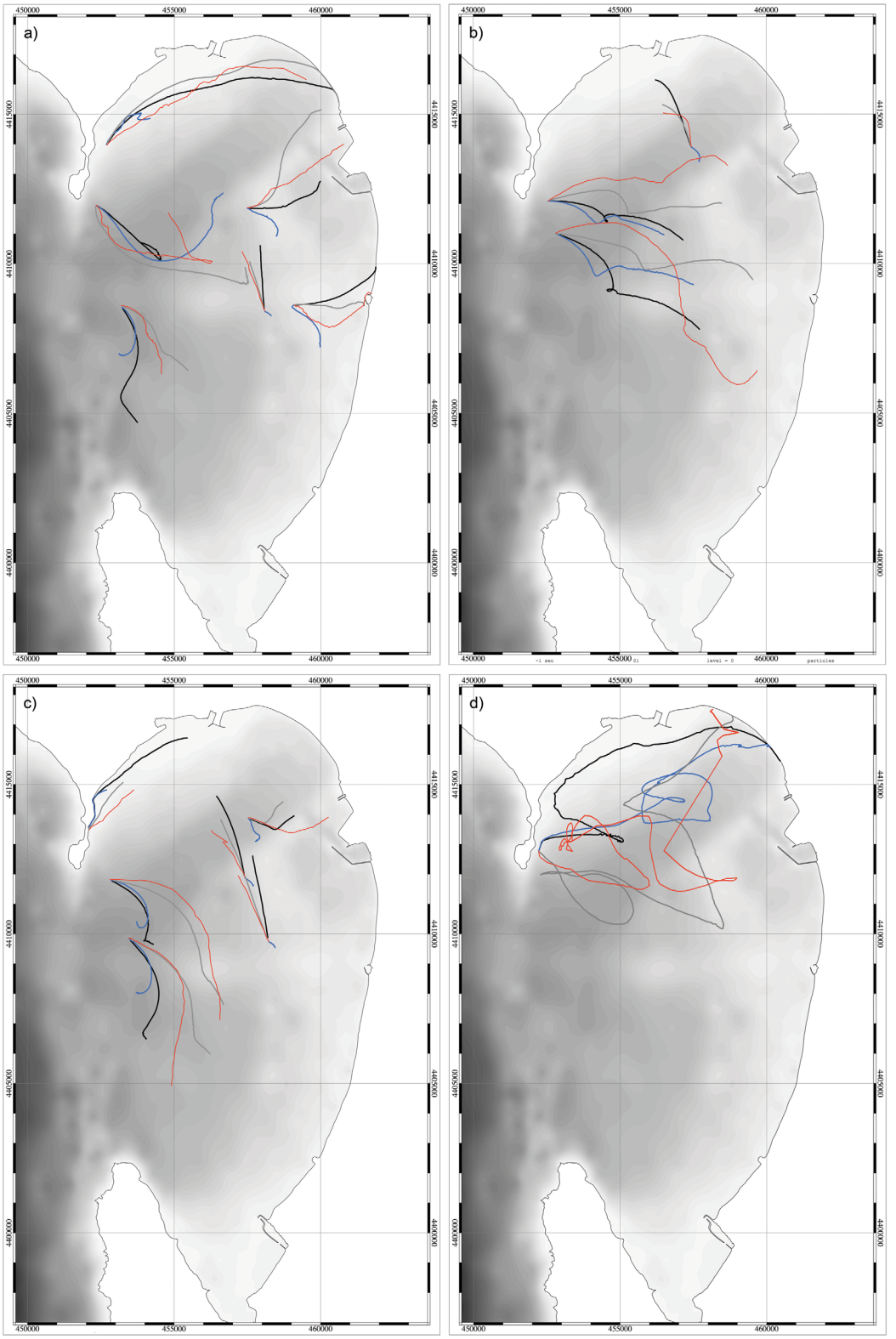

Figure 7. Observed and simulated trajectories of the whole set of released drifters. For sake of clarity the paths are illustrated using four different panels without any separation between winter and summer measurements. Red lines represent the observed trajectories. Gray lines represent the WMS scenario results; black lines and blue lines refer to scenario results obtained using ECMWF and SKIRON wind data, respectively. The paths represent the average trajectories followed by each group of particles released at each drifter starting positions. Gray colors represent a proxy of the Gulf bathymetry, which is depicted in detail in Figure 1b.

Table 1. Statistics of the Lagrangian Current Speeds, Expressed in m/s[a]

	AVG_t	AVG_s	AVG_w	MAX_s	MAX_w
OBS	0.11	0.10	0.12	0.32	0.53
WMS	0.09	0.09	0.10	0.24	0.19
ECMWF	0.08	0.09	0.08	0.23	0.21
SKIRON	0.05	0.04	0.07	0.11	0.24

[a]OBS, as derived from the drifters measurements; WMS, ECMWF, and SKIRON, as estimated from numerical simulations using different wind data forcing; AVG, average values; MAX, maximum values; subscript t, computed for both measuring periods; subscript s, computed for the summer measuring period; subscript w, computed for the winter measuring period.

For all the scenarios, the maximum Lagrangian current speeds were generally underestimated with respect to the observations (see MAX_s and MAX_w in Table 1). This was probably due to the vertical shear of the near-surface velocities, difficult to model by the commonly adopted numerical approach.

Considering the summer period, characterized by lower wind speeds and variability, the accuracy of the numerical predictions increased for the WMS and ECMWF scenarios, with both the average and maximum values similar to the observations (see AVG_s and MAX_s in Table 1). On the other hand, a reduction of the model accuracy was found for the SKIRON scenario.

During the winter period, characterized by higher wind speeds and gustiness, the accuracy of the model results decreased for all the three scenarios, with slightly better results in reproducing the maximum speed values when using SKIRON wind data (see AVG_w and MAX_w in Table 1).

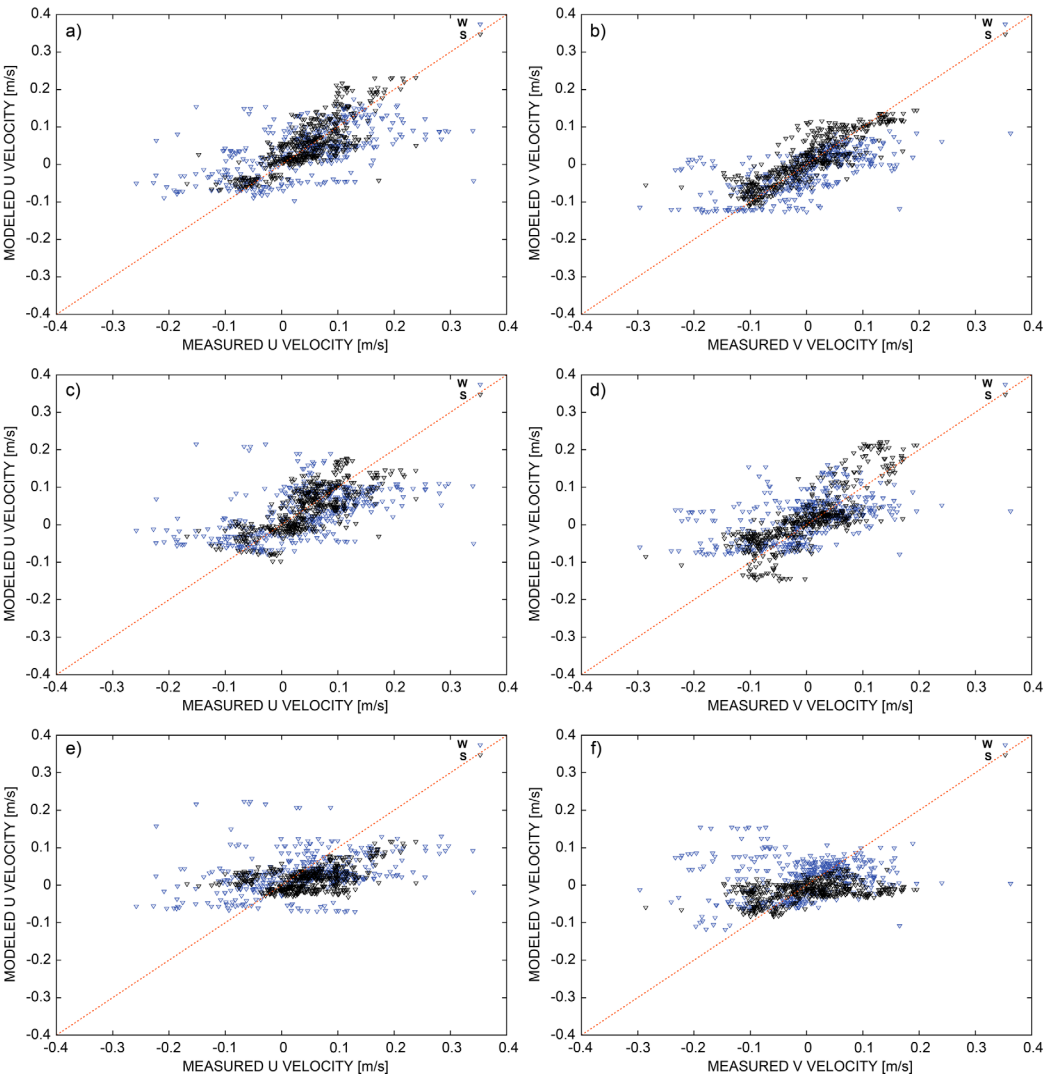

Figure 8. Scatterplots of observed and simulated Lagrangian velocity components: Figures 8a and 8b refer to WMS scenario results; Figures 8c and 8d refer to ECMWF scenario results; Figures 8e and 8f refer to SKIRON scenario results; w and s refer to winter or summer measurements.

Table 2. Comparison Between Observed and Modeled Drifters Horizontal Velocities[a]

	WMS		ECMWF		SKIRON	
	U_{obs}–U_{mod}	V_{obs}–V_{mod}	U_{obs}–U_{mod}	V_{obs}–V_{mod}	U_{obs}–U_{mod}	V_{obs}–V_{mod}
Bias	−0.003	0.0005	0.004	−0.011	0.015	−0.002
ρ	0.66	0.72	0.59	0.62	0.36	0.21
RMSD	0.063	0.055	0.068	0.067	0.079	0.087
S	0.65	0.67	0.57	0.62	0.29	0.24

[a]U and V, drifters velocities components; subscript obs, computed by drifters measurements; subscript mod, estimated by simulations results; Bias expressed in m/s; ρ, Pearson correlation; RMSD, centered root mean square error expressed in m/s; S, skill score.

In Figure 8, the scatterplots of the modeled and observed Lagrangian horizontal velocities are reported for all the three scenarios. The black and blue triangles distinguish the winter measurements from the summer ones.

In Table 2 the Pearson correlation ρ, the Bias, and the centered root mean square error (RMSD) between the three scenarios results and the observations are reported for the velocity horizontal components.

In all the three scenarios the bias was negligible with values around 1 cm/s. For both WMS and ECMWF scenarios, ρ was generally fair indicating a general agreement between the modeled and the observed data sets. The highest correlation, around 0.7, was found, as we expected, for the WMS scenario.

On the contrary, when using SKIRON wind data, the accuracy in reproducing the horizontal Lagrangian velocities was low, with ρ varying between 0.2 and 0.4. This was confirmed also by the RMSD, with the highest discrepancies, corresponding to values higher than 0.08 m/s, found for the SKIRON scenario, whereas RMSD around 0.06 m/s were found for the other two scenarios.

In Figure 9, the Taylor diagrams [*Taylor*, 2001] are reported to summarize the model performances in the three different scenarios. When using SKIRON wind data (blue triangles in Figure 9), the model performances were not satisfactory. In fact, in addition to the low ρ and high RMSD (see Table 2), high discrepancies were also found for the Standard Deviations (STD), with relative differences between the computed and observed velocity components around the 50%. Significantly higher accuracies were found for WMS and ECMWF scenarios (gray stars and black squares in Figure 9), which, along with the higher ρ and low RMSD, the computed STD generally underestimated the observed ones by values ranging between 5 and 20%.

Considering the low differences in RMSD, the skill score S [*Taylor*, 2001] was estimated for the three scenarios (see Table 2) confirming the best model performance, with $S_x = 0.65$ and $S_y = 0.67$, for the WMS scenario, followed by ECMWF with $S_x = 0.57$ and $S_y = 0.62$, and, finally, by SKIRON scenario, with the worst accuracy evidenced by S values always lower than 0.3.

5.2. Observed and Computed Trajectories

In Figure 10 the TRE and TAE are reported for the three scenarios as a function of the prediction time lag, varying between 1 and 24 h.

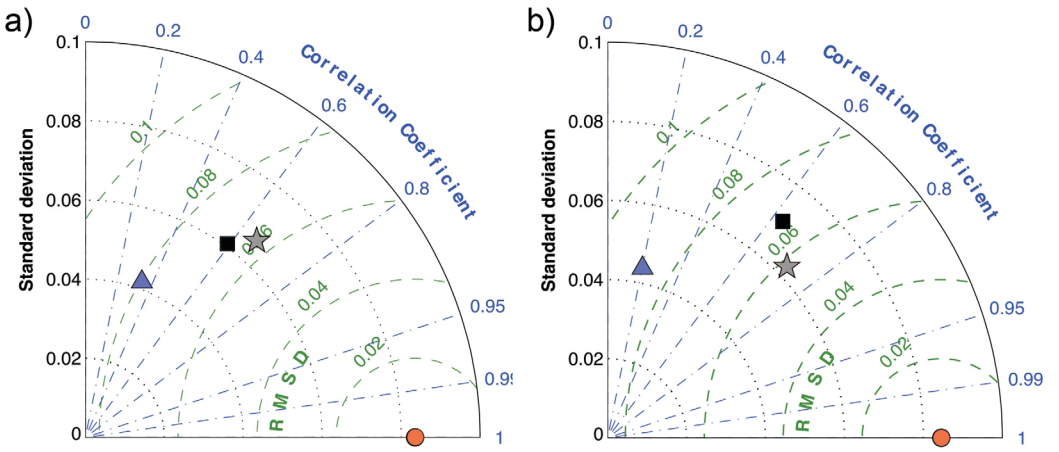

Figure 9. Taylor diagrams for the (a) x and (b) y component of the Lagrangian velocities. Gray stars refer to WMS scenario results. Black squares refer to EMWF scenario results. Blue triangles refer to SKIRON scenario results. Red dots refer to the observations.

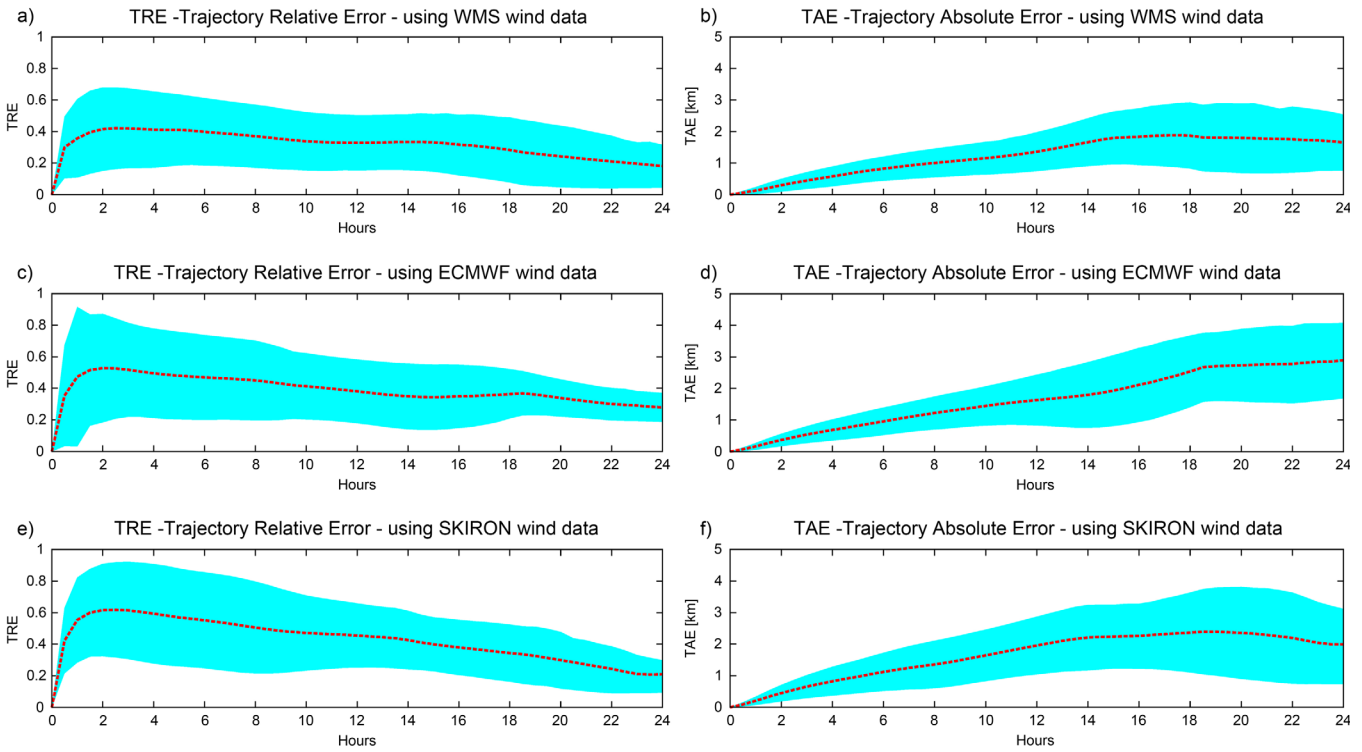

Figure 10. TRE and TAE as a function of the forecast time lag computed for each forcing scenario. Red dashed line indicate average values, shaded area corresponds to the standard deviations. Figures 10a and 10b refer to WMS scenario results; Figures 10c and 10d refer to ECMWF scenario results; Figures 10e and 10f refer to SKIRON scenario results.

In the WMS scenario, the average TRE (red dashed line in Figure 10a) increased with the time within the first 3 h up to a value of 0.41 then slightly decreasing down to 0.17 at the 24th hour. On the other hand, the average TAE (Figure 10b) increased almost linearly up to a maximum average displacement (red dashed line) of about 1.9 km at the eighteenth hour and settling around 1.6 km at the 24th hour.

When using ECMWF wind data (see Figures 10c and 10d), the highest average TRE was found after the first 4 h with a value of 0.52. Then, the TRE decreased with the prediction time down to 0.27 at the 24th hour. The TAE increased almost linearly up to a maximum average displacement of 2.8 km found at the 24th hour.

In the SKIRON scenario (see Figures 10e and 10f), the average TRE increased during the first 3 h reaching a peak value of 0.63 then reducing to 0.2 after the first day of prediction. The TAE increased up to a maximum average displacement of about 2.4 km at the nineteenth hour of prediction then slightly decreasing to values of about 2 km.

In Table 3 a summary of the average values of both TRE and TAE computed at the 1st, 6th, 12th, and 24th hour from the initial release are reported for each scenario. For similar applications, using surface current fields measured by HF radars in coastal and shelf areas, the estimated TAE at the 24th hour ranged between 3.5 and 7 km [*Ullman et al.*, 2006; *Abascal et al.*, 2009a; *Molcard et al.*, 2009; *Berta et al.*, 2014]. If compared with the results obtained from the three scenarios, the estimated model accuracy was largely satisfactory with an average displacement, after 1 day from the release, varying between 1.6 and 2.9 km (see Table 3).

As for the previous analysis, an accuracy index was defined to rank the three scenarios. The average of the TRE computed within the first 6 h from the release (TRE6) was selected. The choice of this time interval was made being the Lagrangian predictability time scales always associated, in literature, with values lower than 24 h [*Sammari et al.*, 1995; *Bauer et al.*, 1998; *Berta et al.*, 2014].

The obtained values distinguished the WMS scenario results as the most accurate, with a TRE6 = 0.39, followed by the ECMWF scenario, with a TRE6 = 0.47 and, finally by SKIRON scenario, with a TRE6 = 0.59. Hypothesizing the drifters following linear trajectories characterized by homogeneous and constant

Table 3. Uncertainties of Model-Predicted Trajectories in the Three Scenarios[a]

	Err. Typ	1st	6th	12th	24th	TRE_6
WMS	TAE	131	823	1362	1656	0.39
	TRE	0.35	0.39	0.32	0.18	
ECMWF	TAE	162	956	1632	2890	0.47
	TRE	0.47	0.46	0.38	0.27	
SKIRON	TAE	202	1118	1956	1998	0.59
	TRE	0.55	0.55	0.45	0.20	

[a]TAE, TRE, trajectory absolute error, expressed in meters (see equation (1)) and trajectory relative error (see equation (2)), computed for the WMS, ECMWF, and SKIRON scenarios at the 1st, 6th, 12th, and 24th hours from the release; TRE6, averaged TRE values computed within the first 6 h from the release.

displacement velocities, the obtained TRE6 values indicated maximum deviation angles between the simulated trajectories and the hypothetical reference paths of 21° in the WMS, of 24° in the ECMWF and of 30° in the SKIRON scenario.

The comparison of the three scenarios results and the consequent ranking of the model performances have proved to be independent from the adopted model parameters setup. A sensitivity analysis of the accuracy of the simulations results in relation to the use of different set of model parameters values was carried out and the results reported in Appendix C. The analysis indicated that the changes of the model parameters values within their typical ranges of variation affect similarly the accuracy of each scenario results, thus confirming the robustness of the followed approach and the consistency of the previous evaluations.

5.3. Trajectories Predictability

The skill score S and the TRE6 analysis confirmed, as we expected, the WMS wind fields as the most efficient forcing for predicting the Lagrangian surface currents and the drifters trajectories in the Gulf, followed, with a slightly lower accuracy, by the ECMWF predicted wind data and, finally, by the SKIRON wind data set, characterized by the highest discrepancies with the observations.

The two approaches used to define the model accuracy provided, qualitatively, similar results. Nevertheless, the differences between the model accuracy in the three scenarios were not equally estimated by S and TRE6 values. In particular, the S analysis, comparing the horizontal components of the observed and predicted velocity fields, separately, can provide only an indicative evaluation of the model accuracy in reproducing the Lagrangian current fields. On the other hand, the TRE6 analysis, based on the direct comparison of the observed and predicted drifter paths, is more suitable to provide a comprehensive overview of the model error in reproducing the surface transport. Furthermore, for operational purposes, as the ones related to the maritime safety or to the sea-ecosystem integrity (e.g., search and rescue or pollution mitigations operations), one of the most useful information to include when providing a prediction is the area or ray of uncertainty which is basically expressed by the TRE [*Thompson et al*., 2003].

Therefore, considering the TRE6 as a more useful and intuitive proxy of the model accuracy, we found that the WMS scenario was in mean 1.2 times more accurate than the ECMWF scenario and 1.48 times more accurate than SKIRON scenario.

In WMS scenario, the errors in reproducing the observed trajectories can be generated both by the adopted numerical approximations and by the phenomenological assumptions made, excluding other meteo-marine forcings except the wind [*Beg Paklar et al*., 2008].

In particular, the results of the scale analysis reported in Appendix B excluded the nonreproduction of the baroclinic pressure gradients and of the tidal contribution as a main source of errors for the numerical simulations. In addition, even the influence of the open sea general circulation on the local surface transport was considered as negligible.

Therefore, if the WMS wind data are considered as a proper proxy of the real wind in the Gulf area (see section 3.1 and Appendix C), the main source of errors in the WMS scenario can be associated to the numerical reproduction of the ocean surface boundary layer, specifically to the adopted model vertical discretization and parameterization of the vertical energy fluxes. In fact, as suggested by *Carniel et al*. [2009], the accurate reproduction of the density stratification at the ocean surface, fundamental for modeling the transfer of momentum from the atmosphere to the ocean, is one of the major factor affecting the predictability of the surface transport at sea.

We also investigated the role of the wind variability within the Gulf as a potential factor influencing the accuracy of the model results. A numerical simulation was performed using, as wind forcing, the time series of the

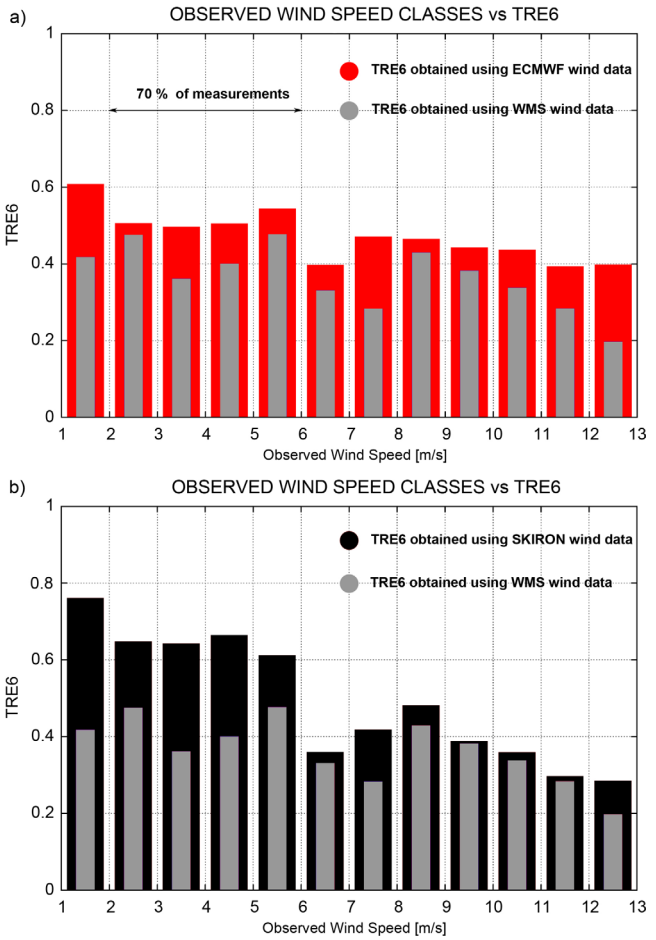

Figure 11. TRE6 as a function of the observed wind speed classes. (a) Comparison between ECMWF (red bars) and WMS (gray bars) scenario results; (b) comparison between SKIRON (black bars) and WMS (gray bars) scenario results.

wind speeds and directions obtained from the spatial averages of the WMS wind fields. The accuracy of the obtained results, with a TRE6 = 0.41, was only slightly lower than the one of the WMS scenario but always higher than the accuracy of the ECMWF and SKIRON scenarios (see Table 2). This indicated that the reproduction of the spatial features of the wind fields in the Gulf is important but not fundamental for an accurate reproduction of the sea surface transport in the area. As a consequence, it follows that the role of the different mesh spatial resolution of the two WPS was important mainly for the prediction of the temporal variability of the wind speeds and directions more than for the reproduction of the wind spatial variability within the Gulf area.

Comparing the ECMWF and SKIRON scenarios, when using the ECMWF wind data, the model accuracy was generally higher for prediction time lags lower than 16–18 h. On the contrary, an inverse behavior, with higher accuracy for SKIRON scenario and lower for ECMWF, was detected for temporal intervals higher than 18–20 h (see Figures 10c–10f and Table 3). These differences can be only related to the differences in the accuracy of the adopted wind fields. Considering that most of the drifters trajectories lasting more than 20 h were observed during the winter experiment, which was characterized by higher wind speeds, the variability of the TRE6 was investigated with respect to the wind speed classes.

For each scenario, the TRE6 was computed in relation to 12 selected wind speed classes varying between 1 and 13 m/s. In particular, the TRE6 values, estimated for each prediction time lag, were grouped in relation to the observed wind speed measured at the time of computation. Then, for each observed speed class, the average TRE6 was calculated.

In Figures 11a and 11b, the set of values obtained from ECMWF and SKIRON scenarios (red bars for ECMWF and black bars for SKIRON) were compared with ones from the WMS scenario (gray bars).

As we expected, for WMS scenario, the TRE6 was the lowest for all the considered wind speed classes. It ranged between 0.47 and 0.19 with a low variability, around 0.08 of STD, but with a marked decreasing trend for speed classes higher than 8 m/s. These latter values only slightly influence the overall average TRE6 being most of the measurements included between 2 and 6 m/s (see Figure 4) of wind speeds. This is in line with the results obtained by other studies expecting a better match between model results and observations for higher current speeds [*Thompson et al*., 2003; *Spydell et al*., 2015]. In fact, as stated by *Yaremchck et al*. [2013], the higher the background flows the lower the horizontal shears which is a dynamical condition favoring the numerical reproduction of the sea surface transport.

In ECMWF scenario (Figure 11a), the TRE6 ranged between 0.61 and 0.39 with a standard deviation of 0.06. The TRE6 varied homogeneously in relation to the wind speeds, with slightly higher values found for the lower wind speed class.

On the contrary, for SKIRON scenario (Figure 11b), the TRE6 strongly decreased with increasing wind speeds. The values ranged between 0.78, for wind speeds comprised between 1 and 2 m/s, and 0.27 for wind speeds higher than 12 m/s, thus indicating a strong dependency of the model accuracy on the speed classes, when using SKIRON wind data.

In Figure 12, the relative differences between the TRE6 computed for ECMWF and SKIRON scenario and the TRE6 computed for WMS scenario (TRE6_RD) were reported for each wind speed class. The TRE6_RD computed by the following equation:

$$TRE6_R D^{WPS} = \left(TRE6^{WPS} - TRE6^{WMS}\right)/TRE6^{WMS}, \quad (3)$$

with superscript WPS indicating the SKIRON or ECMWF scenario data, allowed to remove the systematic errors due to the inaccuracies of the hydrodynamic and trajectory model and to quantify only the errors generated by the type adopted wind forcing.

Despite the previous evaluations based on the TRE6 analysis, the behavior of the TRE6_RD with respect to the observed wind speed classes highlighted the presence of trends for both scenarios (see Figure 12).

In SKIRON scenario (black dashed line in Figure 12), the tendency of the accuracy to increase with the measured wind speeds was found. The TRE6_RD decreased from around 80% for low speed values to around 5% for wind speed classes between 11 and 12 m/s, to increase again up to around 40% for the highest wind speeds. On the other hand, for ECMWF scenario (red line in Figure 12) the trend was the opposite with less relative increments in the model errors found at lower wind speeds and higher for high wind speed classes. In this case the TRE6_RD ranged between around 40% at low wind speeds and around 100% at the highest values.

Therefore, for wind speed classes between 1 and 6 m/s the use of ECMWF wind data was preferable for reproducing the drifters paths in the Gulf then, between 6 and 8 m/s both WPS produced similar errors in the model results and, finally, for wind speeds higher than 8 m/s the use of SKIRON wind data increased the model accuracy.

Considering the type of adopted wind forcing as the only source of model error, the Vectorial Differences (VD) between the hourly fields of observed wind data and the hourly fields of predicted ones were estimated for both WPS data sets following the equation:

$$VD^{WPS} = \left\langle \sqrt{\left[\left(w_x^{WPS} - w_x^{WMS}\right)^2 + \left(w_y^{WPS} - w_y^{WMS}\right)^2\right]} \right\rangle_{np}, \quad (4)$$

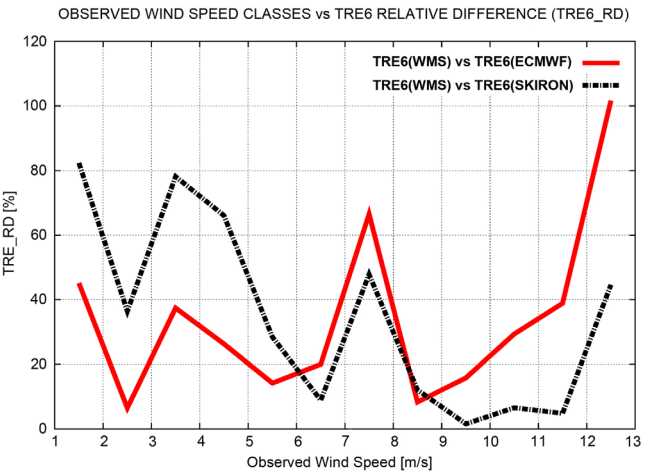

Figure 12. TRE6_RD as a function of the wind speed classes. Red line indicates the TRE6 relative differences between ECMWF scenario results and WMS scenario results. Black dashed line indicates the TRE6 relative differences between SKIRON scenario results and WMS scenario results.

with w_x and w_y the computed (superscript WPS) and observed (superscript WMS) wind speed components, and n p the number of nodes of each WPS reduced domain (see Figure 2). The VD quantifies the uncertainties of both the modules and directions of the predicted wind velocity vectors, which is fundamental when considering the transport process. In Figure 13, the VD is reported as a function of the wind speed class and for the two WPS separately.

The two types of predicted wind data showed different trends of the VD with respect to the increment of the wind speed, with the discrepancies from the observations increasing in the case of ECMWF and decreasing in the case of SKIRON.

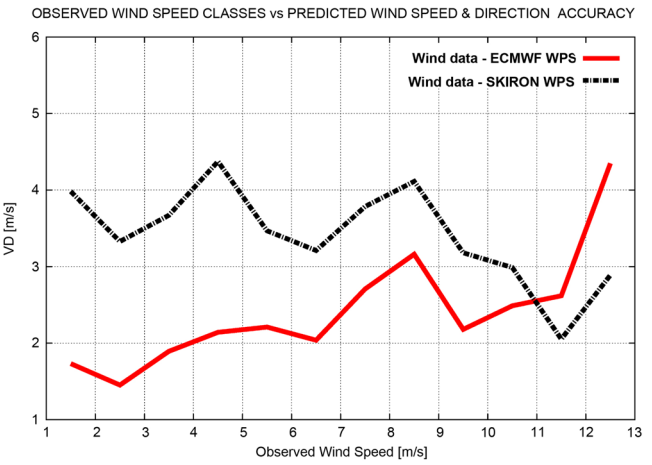

Figure 13. Average amplitude of Vectorial Differences (VD) between WMS vector fields and predicted data in relation to the wind speed classes. Red line refers to the VD between WMS and ECMWF wind fields; black dashed line refers to the VD between WMS and SKIRON wind fields.

These differences can occur from a number of reasons and their exact identification is beyond the scope of this paper. Nevertheless, the SKIRON WPS, characterized by a higher spatial resolution and by taking into account the nonhydrostatic processes, was probably more efficient in reproducing the orographic effects on the wind generation processes. In particular, the Mistral wind, which characterizes the most intense events during the winter experiment, is influenced, at subbasin scale, by the interaction between the synoptic scale flow and the orography. As for other typical intense wind regimes, as the bora in the Adriatic Sea, the positive effects on oceanographic modeling of higher-resolution atmospheric forcing was recognized by many authors [*Pullen et al*., 2003; *Kuzmić et al*., 2006]. However, as stated by *Beg Paklar et al*. [2008], the use of higher spatial resolution in atmospheric forcings not always ensures a better accuracy of the simulated winds. This is mainly due to the negative effects generated by the nesting procedure that can reduce the precision of the results and that was evidenced by the overall lower accuracy of the SKIRON data set.

On the other hand, the ECMWF WPS, characterized by lower spatial resolution and by the absence of nesting procedure, was less accurate on reproducing the peak speeds but more accurate in reproducing the evolution of the meso-scale phenomena, which dominates the low and medium wind speed ranges characterizing most of the investigated periods.

While the variability of the TRE6_RD (see Figure 12) and of the VD (see Figure 13) in relation to the wind speed classes was coherent, the switch between higher and lower accuracies between the two scenarios was not exactly predicted by these two data sets. This revealed the impossibility of defining a simple transfer function linking the errors in predicting the sea surface transport and the errors in predicting the wind fields, which could be valid for all the wind speed classes.

Nevertheless, considering the intervals of wind speed between 1 and 6 m/s, characterizing most of the drifters measurements, the TRE6_RD and the VD varied coherently in both scenarios. For these intervals, the two data set were compared one each other in order to quantify the amplification of the error in reproducing the sea surface transport generated by the uncertainties in the predicted wind fields. Simple linear correlation between the TRE6_RD and the VD data sets revealed that to an error of 1 m/s in the predicted wind, as estimated by the VD, corresponded a reduction of the accuracy in the sea surface transport prediction, as estimated by the TRE6_RD, of about the 15% with a variability of $\pm$3%.

6. Concluding Remarks

The accurate prediction of the wind-induced sea surface transport in coastal areas using numerical modeling techniques is strongly dependent on the accuracy of the adopted wind forcing. The use of wind data set obtained from different weather prediction systems can promote an increase or a reduction of the trajectories prediction accuracy.

We tested two different weather prediction systems, ECMWF and SKIRON, using the predicted wind data as forcing for a hydrodynamic and particles-tracking model applied to reproduce a set of observed drifters trajectories in a specific coastal area of the Mediterranean Sea, the Gulf of Oristano.

The simultaneous implementation of a wind measuring system, constituted by a set of anemometers located along the coastline and in the mainland, allowed to estimate the real wind fields in the Gulf. Although

the wind fields derived from the anemometric data are still an estimate of the real winds in the Gulf, they represent a proper proxy [*Zecchetto et al*., 2016].

The observed anemometric data were used as a reference data set for testing the accuracy of the hydrodynamic and particle-tracking model results when using ECMWF and SKIRON wind as forcing. In similar studies, this type of evaluation was generally carried out without an a priori estimate of the systematic errors of the numerical model, therefore without the possibility of correctly quantifying the errors generated by the type of adopted wind forcing [*Beg Paklar*, 2008; *Brushett et al*., 2011; *Brushett et al*., 2016].

Specific Lagrangian metrics (TRE and TAE) were defined to estimate the accuracy of the different model configurations in reproducing the observed drifter paths in relation to different forecasting time lags.

The results revealed that the model accuracy using the observed wind data (WMS scenario) was suitable for most of the operational oceanographic purposes, such as the ones related to the maritime safety or to the sea-ecosystem integrity. This reference was used to quantify the discrepancies of the model results from the observations produced by the use of ECMWF and SKIRON wind data as model forcing.

The accuracy of the model results using the predicted wind fields decreased between 1.2 and 1.5 times with respect to the reference scenario. In particular, ECMWF data were generally more efficient as model forcing to predict the drifters trajectories, with results about 3 times more accurate than the ones obtained using SKIRON data.

The analysis also demonstrated that the accuracy of the simulation results using the wind data predicted by the two WPS was strongly dependent on the observed wind speed intensities. For wind speed classes higher than 6 m/s, the use of SKIRON data was promoting the accuracy of the model solutions, whereas for lower wind speed classes the ECMWF data were preferable as model forcing.

The increments of the errors in the model solutions in relation to the wind speed class were highly variable for both ECMWF and SKIRON scenario. The values ranged between 5 and 100%, therefore evidencing the difficulty of defining the most efficient wind data set in absolute.

Although an error transfer function between the prediction of the sea surface transport and the prediction of the wind, valid for all the speed classes, could not be assessed, nonetheless, for wind speeds lower than 6 m/s, characterized by a coherent behavior between TRE6_RD and VD, and including most of the Lagrangian measurements, it could be defined. In fact, for such speed intervals, the amplification of the errors in predicting the sea surface transport produced by a discrepancy of the predicted wind data of 1 m/s was estimated to be around the 15%.

In ocean modeling, various procedures, including simple or constant multiplicative factors or more complex linear regression functions, are often used to correct the systemic bias of the numerical results from the observations [*Brenner et al*., 2007; *Durrant et al*., 2013]. The obtained results revealed that no fixed rules acting directly on the wind forcing could be assessed as a proper solution to improve the accuracy of the numerical prediction of the sea surface transport in coastal areas.

Concluding, due to the uncertainties of the operational atmospheric models in reproducing a realistic wind field at coastal scale [*Accadia et al*., 2007; *Zecchetto and Accadia*, 2014], the implementation of a wind measuring system would be always desirable for ocean model applications in coastal seas. In fact, the measured anemometric data can be adopted both for evaluating the accuracy of the atmospheric forcings used to make the ocean predictions and for an efficient calibration of the numerical ocean model itself. Finally, the proposed approach, based on the implementation of a wind measuring system, Lagrangian observations and numerical reproduction of the sea surface transport, is highly replicable and it can be adapted to different coastal areas, providing significant benefit for the understanding of primarily wind-driven coastal dynamics.

Appendix A: The Hydrodynamic and Particle-Tracking Model

SHYFEM is a three-dimensional hydrodynamic model based on the finite element method which resolves the shallow water equations integrated over each layer in their formulations with water levels and transports. It uses finite elements for horizontal spatial discretizations, z-layers for vertical discretizations, and a semi-implicit algorithm for integration in time.

It accounts for barotropic, baroclinic, and atmospheric pressure gradients as well as wind drag and bottom friction, nonlinear advection, and vertical turbulent processes. The solved equation system reads as

$$\frac{\partial U_l}{\partial t}+Adv_l^x-fV_l=gh_l\frac{\partial \zeta}{\partial x}-\frac{gh_l}{\rho_0}\frac{\partial}{\partial x}\int_{-H_l}^{\zeta}\rho' dz+\frac{h_l}{\rho_0}\frac{\partial p_a}{\partial x}+\frac{1}{\rho_0}\left(\tau_x^{top(l)}-\tau_x^{bottom(l)}\right)+A_H\left(\frac{\partial^2 U_l}{\partial x^2}+\frac{\partial^2 U_l}{\partial y^2}\right)$$

$$\frac{\partial V_l}{\partial t}+Adv_l^y+fU_l=gh_l\frac{\partial \zeta}{\partial y}-\frac{gh_l}{\rho_0}\frac{\partial}{\partial y}\int_{-H_l}^{\zeta}\rho' dz+\frac{h_l}{\rho_0}\frac{\partial p_a}{\partial y}+\frac{1}{\rho_0}\left(\tau_y^{top(l)}-\tau_y^{bottom(l)}\right)+A_H\left(\frac{\partial^2 V_l}{\partial x^2}+\frac{\partial^2 V_l}{\partial y^2}\right) \quad \text{(A1)}$$

$$\frac{\partial \zeta}{\partial t}+\sum_l\frac{\partial U_l}{\partial x}+\sum_l\frac{\partial V_l}{\partial y}=0,$$

where l indicates the vertical layer, (U_l, V_l) the horizontal transport components in x and y directions for each layer, Adv^x and Adv^y the advective terms, p_a the atmospheric pressure, g the gravitational acceleration, f the Coriolis parameter, ζ the water level, ρ_0 the standard water density, $p=p_0+p'$ the water density, h_l the layer thickness, H_l the depth of the bottom of the layer l, A_h the horizontal eddy viscosity. For the computation of the vertical diffusivities and viscosities, the General Ocean Turbulence Model (GOTM) described in *Burchard and Petersen* [1999] was used.

Wind and bottom friction terms, corresponding to the boundary conditions of the stress terms (τ_x, τ_y), are defined as

$$\begin{aligned}\tau_x^{surface}&=c_D\rho_a w_x\sqrt{w_x^2+w_y^2}\\ \tau_x^{bottom}&=c_B\rho_0 u_L\sqrt{u_L^2+v_L^2}\\ \tau_y^{surface}&=c_D\rho_a w_y\sqrt{w_x^2+w_y^2}\\ \tau_y^{bottom}&=c_B\rho_0 v_L\sqrt{u_L^2+v_L^2},\end{aligned} \quad \text{(A2)}$$

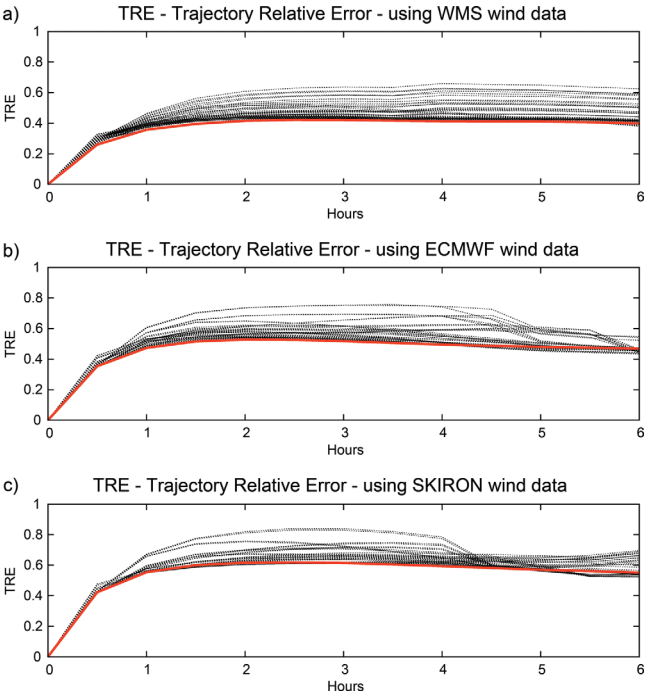

Figure A1. TRE computed for (a) WMS, (b) ECMWF, and (c) SKIRON scenario as a function of a forecasting time lag varying between 0 and 6 h. Dashed black lines describe the variability of TRE obtained from a subset of selected simulations characterized by different combination of the model parameters values. Red continuous lines refer to TRE computed from the simulations results using the set of model parameters values maximizing the accuracy of the WMS scenario results.

with C_D as the wind drag coefficient set to 2.9×10^{-3}, C_B the bottom friction coefficient set to 2.5×10^{-3}, ρ_a the air density (w_x, w_y) the wind velocity components, and (u_L, v_L) the bottom velocity components.

The hydrodynamic model is coupled with a particles trajectories module that solves the advection and diffusion equation in a Lagrangian framework of reference

$$\begin{aligned}\frac{\partial x}{\partial t}&=u_a+u_d\\ \frac{\partial y}{\partial t}&=v_a+v_d,\end{aligned} \quad \text{(A3)}$$

where u_a, v_a are the advective velocities components and u_d, v_d are the diffusive velocities components in x and y directions, respectively.

The components u_a and v_a are expressed as

$$\begin{aligned}u_a&=C_c u_1+C_w w_x\\ v_a&=C_c v_1+C_w w_y,\end{aligned} \quad \text{(A4)}$$

where u_1, v_1 are the Eulerian velocities computed by the hydrodynamic model for the first vertical layer; w_x, w_y are

the wind velocity components measured by the WMS or computed by the two WPS; C_c and C_w are the water current transport factor and the wind drift factor set to 0.9 and 5×10^{-3}, respectively.

The horizontal components of the turbulent diffusive velocities, u_d and v_d, were computed using a random walk technique on the basis of the *Fischer et al*. [1979] study, with turbulent diffusion coefficients obtained using the Smagorinsky formula [*Smagorinsky*, 1993].

The adopted numerical method for solving equation (A3) is based on the finite elements and it is not subjected to any constrain for the selection of the proper computational time step.

Appendix B: Scale Analysis

A simple-scale analysis was performed to evaluate the weight of the baroclinic contribution on the total momentum for the addressed case study.

We assumed that the differences in the Gulf water densities were generated by water temperature gradients only, being the freshwater inputs negligible (see section 2), and that the differences between the surface temperatures were representative of the temperature differences along the whole water column, which is acceptable for shallow water areas relatively isolated from the open sea dynamic (see section 2).

Following the approach proposed in *Umgiesser et al*. [2004], the wind stress term (A) and the baroclinic pressure gradients term (B) in equation (A1) were integrated over the total water depth H, obtaining, along the x direction

$$A=\frac{\tau}{H\rho}=\frac{C_D\rho_a w_x^2}{H\rho}, \tag{B1}$$

$$B=\frac{gH}{2}\frac{1}{\rho}\frac{d\rho}{dx}=\frac{gH}{2}\alpha\frac{\Delta T}{L}, \tag{B2}$$

with ρ the vertical average water density, ΔT the spatial difference of the water temperatures, L the characteristic length scale, α the thermal coefficient of expansion with a typical value of 2×10^{-4}, C_D the wind drag coefficient set to 2.9×10^{-3}, ρ_a and ρ the air and water density, w the wind speed, and g the gravitational acceleration.

The two terms A and B were compared one each other for the summer experiment, characterized by the highest differences in T and by the lower wind intensities (see section 4.1). We obtained that the momentum induced by a wind speed of 5 m/s, the typical summer speed intensity, acting on a water column of 12 m, corresponding to the average Gulf depth, was around 8 times more intense than the baroclinic contribution generated by a difference in temperature of 0.4°C measured by the drifters over a distance of 5 km (see section 4.1).

Considering that the wind is a surface forcing, its relative contribution to the sea surface transport should be even an order of magnitude higher than the value obtained assuming it as acting homogeneously along the whole water column.

Therefore, for both summer and winter experiments, the contribution of the baroclinic pressure gradients in the momentum equation was negligible.

Appendix C: The Model Sensitivity Analysis

A sensitivity analysis was carried out to define the role of the numerical model parameterizations on the trajectories prediction accuracy. A set of numerical simulations were performed to reproduce the drifters trajectories using, as forcing, the three different types of wind data as described in section 4.2.2.

At each model run, the values of C_D in equation (A2), C_w and C_c in equation (A4), which are the main model parameters influencing the reproduction of the sea surface transport, were changed within their typical ranges of values, corresponding to 2×10^{-3} and 3×10^{-3} for the C_D, to 1×10^{-3} and 1×10^{-2} for the C_w, and to 0.8 and 1.2 for C_c [*Castanedo et al*., 2006; *Abascal et al*., 2009b; *Wang and Shen*, 2010; *Cucco et al*., 2012b]. The results obtained from each model run were compared with measurements and TRE (see equation (2)) and TRE6 (see section 5.2) computed.

In Figure A1, the TRE computed for each forcing scenario is reported for the first 6 h of predictions and for a subset of selected simulations performed during the sensitivity analysis. Specifically, black lines in Figure A1 refer to the TRE obtained from a total of 27 simulations characterized by a combination of parameters values varying among the minimum, the maximum and the average of each range. In addition, the red continuous lines in Figure A1 indicate the accuracy of the model results obtained using the combination of parameters values minimizing the TRE6 in the WMS scenario, corresponding to $C_D = 2.9 \times 10^{-3}$, $C_c = 0.9$, and $C_w = 5 \times 10^{-3}$, and that have been considered for the discussion.

For WMS scenario, TRE6 varied between 0.39, as computed from TRE values individuated by the red line in Figure A1a, and 0.56 for the worst case with average values of 0.44. In EMCWF scenario, TRE6 varied between 0.47 and 0.65 with average value of 0.53, whereas in SKIRON scenario, TRE6 varied between 0.59 and 0.69 for the worst case, with average of 0.63.

For ECMWF and SKIRON scenarios (Figures A1b and A1c) the differences between the minimum TRE6 and the one computed from TRE values indicated by the red lines are negligible, being around 10^{-3}. Therefore, the combination of parameters values increasing the accuracy of WMS scenario results produces similar effects even for ECMWF and SKIRON scenarios.

The sensitivity analysis highlighted the coherent behavior between the increments of the TRE and TRE6 in the three scenarios in relation to the different combination of the model parameters values. As a consequence, the differences between the accuracies of the simulations results in the three scenarios are basically independent from the adopted parameterization. This behavior is due to the deterministic essence of the adopted numerical model and confirms that the WMS wind data are proper proxy of the real winds in the Gulf and that the ECMWF and SKIRON wind data sets are basically less accurate reproductions, independently from the adopted numerical model setup.

In this study, the values of the model parameters were set to maximize the accuracy of the simulation results in order to efficiently highlight the errors generated by the adopted type of wind forcing.

Acknowledgments
This research was funded by the Flagship Project RITMARE (SP3-WP4-AZ5)—The Italian Research for the Sea—coordinated by the Italian National Research Council and funded by the Italian Ministry of Education, University and Research within the National Research Program 2011–2013. The authors wish to thank the Oristano Coastguard, the Sinis MPA, and the staff of the National Air Force Base of Capo Frasca for the logistic and technical support. The authors would also like to thank the National and Kapodistrian University of Athens and the European Centre for Medium-Range Weather Forecasts (ECMWF) for the wind data. The data in figures and tables can be acquired by contacting the author via e-mail: andrea.cucco@cnr.it.

References

Abascal, A. J., S. Castanedo, R. Medina, I. J. Losada, and E. Alvarez-Fanjul (2009a), Application of HF radar currents to oil spill modelling, *Mar. Pollut. Bull.*, *58*(2), 238–248, doi:10.1016/j.marpolbul.2008.09.020.

Abascal, A. J., S. Castanedo, F. J. Mendez, R. Medina, and I. J. Losada (2009b), Calibration of a Lagrangian transport model using drifting buoys deployed during the prestige oil spill, *J. Coastal Res.*, *25*, 80–90, doi:10.2112/07-0849.1.

Accadia, C., S. Zecchetto, A. Lavagnini, and A. Speranza (2007), Comparison of 10-m wind forecasts from a regional area model and QuikSCAT scatterometer wind observations over the Mediterranean Sea, *Mon. Weather Rev.*, *135*(5), 1945–1960, doi:10.1175/MWR3370.1.

Alves, T. M., E. Kokinou, G. Zodiatis, and R. Lardner (2015), Hindcast, GIS and susceptibility modelling to assist oil spill clean-up and mitigation on the southern coast of Cyprus (Eastern Mediterranean), *Deep Sea Res., Part II*, doi:10.1016/j.dsr2.2015.07.017, in press.

Agüera-Pérez, A., J. C. Palomares-Salas, J. J. González de la Rosa, J. G. Ramiro-Leo, and A. Moreno-Muñoz (2012), Basic meteorological stations as wind data source: A mesoscalar test, *J. Wind Eng. Ind. Aerodyn.*, *107–108*, 48–56, doi:10.1016/j.jweia.2012.03.020.

Bauer, S., M. S. Swenson, A. Griffa, A. J. Mariano, and K. Owens (1998), Eddy-mean flow decomposition and eddy-diffusivity estimates in the tropical Pacific Ocean: 1. Methodology, *J. Geophys. Res.*, *103*(C13), 30,855–30,871, doi:10.1029/1998JC900009.

Beg Paklar, G., N. Žagar, M. Žagar, R. Vellore, D. Koračin, P.-M. Poulain, M. Orlić, I. Vilibić, and V. Dadić (2008), Modeling the trajectories of satellite-tracked drifters in the Adriatic Sea during a summertime bora event, *J. Geophys. Res.*, *113*, C11S04, doi:10.1029/2007JC004536.

Berta, M., L. Bellomo, M. G. Magaldi, A. Griffa, A. Molcard, J. Marmain, M. Borghinia, and V. Taillandier (2014), Estimating Lagrangian transport blending drifters with HF radar data and models: Results from the TOSCA experiment in the Ligurian Current (North Western Mediterranean Sea), *Prog. Oceanogr.*, *128*, 15–29, doi:10.1016/j.pocean.2014.08.004.

Blanke, B., S. Speich, G. Madec, and K. Döös (2001), A global diagnostic of interocean mass transfers, *J. Phys. Oceanogr.*, *31*(6), 1623–1632, doi:10.1175/1520-0485(2001)031 < 1623:AGDOIM>2.0.CO;2.

Brenner, S., I. Gertman, and A. Murashkovsky (2007), Preoperational ocean forecasting in the southeastern Mediterranean Sea: Implementation and evaluation of the models and selection of the atmospheric forcing, *J. Mar. Syst.*, *65*(1–4), 268–287, doi:10.1016/j.jmarsys.2005.11.018.

Brocchini, M., M. Wurtele, G. Umgiesser, and S. Zecchetto (1995), Calculation of a mass-consistent two-dimensional wind field with divergence control, *J. Appl. Meteorol.*, *34*(11), 2543–2555, doi:10.1175/1520-0450(1995)034 < 2543:COAMCT>2.0.CO;2.

Brushett, B. A., B. A. King, and C. J. Lemckert (2011), Evaluation of met-ocean forecast data effectiveness for tracking drifters deployed during operational oil spill response in Australian waters, *J. Coastal Res.*, *64*, 991–994.

Brushett, B. A., B. A. King, and C. J. Lemckert (2016), Assessment of ocean forecast models for search area prediction in the eastern Indian Ocean, *Ocean Modell.*, *97*, 1–15, doi:10.1016/j.ocemod.2015.11.002.

Burchard, H., and O. Petersen (1999), Models of turbulence in the marine environment—A comparative study of two-equation turbulence models, *J. Mar. Syst.*, *21*(1–4), 29–53, doi:10.1016/S0924-7963(99)00004-4.

Caballero, A., M. Espino, Y. Sagarminaga, L. Ferrer, A. Uriarte, and M. González (2008), Simulating the migration of drifters deployed in the Bay of Biscay, during the prestige crisis, *Mar. Pollut. Bull.*, *56*(3), 475–482, doi:10.1016/j.marpolbul.2007.11.005.

Carniel, S., J. C. Warner, J. Chiggiato, and M. Sclavo (2009), Investigating the impact of surface wave breaking on modeling the trajectories of drifters in the northern Adriatic Sea during a wind-storm event, *Ocean Modell.*, *30*(2–3), 225–239, doi:10.1016/j.ocemod.2009.07.001.

Castanedo, S., R. Medina, I. J. Losada, C. Vidal, F. J. Méndez, A. Osorio, J. A. Juanes, and A. Puente (2006), The prestige oil spill in Cantabria (Bay of Biscay). Part I: Operational forecasting system for quick response, risk assessment, and protection of natural resources, *J. Coastal Res.*, *22*, 1474–1489, doi:10.2112/04-0364.1.

Cavaleri, L., and L. Bertotti (1997), In search of the correct wind and wave fields in a minor basin, *Mon. Weather Rev.*, *125*(8), 1964–1975.

Cermeño, P., and P. G. Falkowski (2009), Controls on diatom biogeography in the ocean, *Science*, *325*(5947), 1539–1541, doi:10.1126/science.1174159.

Coppa, S., G. A. de Lucia, P. Magni, P. Domenici, F. Antognarelli, A. Satta, and A. Cucco (2013), The effect of hydrodynamics on shell orientation and population density of Pinna nobilis in the Gulf of Oristano (Sardinia, Italy), *J. Sea Res.*, *76*, 201–210.

Cucco, A., and G. Umgiesser (2015), The trapping index: How to integrate the Eulerian and the Lagrangian approach for the computation of the transport time scales of semi-enclosed basins, *Mar. Pollut. Bull.*, *98*(1–2), 210–220, doi:10.1016/j.marpolbul.2015.06.048.

Cucco, A., A. Perilli, G. De Falco, M. Ghezzo, and G. Umgiesser (2006), Water circulation and transport timescales in the Gulf of Oristano, *Chem. Ecol.*, *22*, suppl. 1, S307–S331, doi:10.1080/02757540600670364.

Cucco, A., G. Umgiesser, C. Ferrarin, A. Perilli, D. M. Canu, and C. Solidoro (2009), Eulerian and Lagrangian transport time scales of a tidal active coastal basin, *Ecol. Modell.*, *220*(7), 913–922, doi:10.1016/j.ecolmodel.2009.01.008.

Cucco, A., M. Sinerchia, C. Lefrançois, P. Magni, M. Ghezzo, G. Umgiesser, A. Perilli, and P. Domenici (2012a), A metabolic scope based model of fish response to environmental changes, *Ecol. Modell.*, *237–238*, 132–141, doi:10.1016/j.ecolmodel.2012.04.019.

Cucco, A., M. Sinerchia, A. Ribotti, A. Olita, L. Fazioli, A. Perilli, B. Sorgente, M. Borghini, K. Schroeder, and R. Sorgente (2012b), A high-resolution real-time forecasting system for predicting the fate of oil spills in the Strait of Bonifacio (western Mediterranean Sea), *Mar. Pollut. Bull.*, *64*(6), 1186–1200, doi:10.1016/j.marpolbul.2012.03.019.

Davis, R. E. (1985), Drifter observations of coastal surface currents during CODE: The method and descriptive view, *J. Geophys. Res.*, *90*(C3), 4741–4755, doi:10.1029/JC090iC03p04741.

De Falco, G., M. Baroli, A. Cucco, and S. Simeone (2008), Intrabasinal conditions promoting the development of a biogenic carbonate sedimentary facies associated with the seagrass Posidonia oceanica, *Cont. Shelf Res.*, *28*(6), 797–812, doi:10.1016/j.csr.2007.12.014.

Döös, K., J. Nycander, and A. C. Coward (2008), Lagrangian decomposition of the Deacon cell, *J. Geophys. Res.*, *113*, C07028, doi:10.1029/2007JC004351.

Döös, K., V. Rupolo, and L. Brodeau (2011), Dispersion of surface drifters and model-simulated trajectories, *Ocean Modell.*, *39*(3–4), 301–310, doi:10.1016/j.ocemod.2011.05.005.

d'Ovidio, F., J. Isern-Fontanet, C. López, E. Hernández-García, and E. García-Ladona (2009), Comparison between Eulerian diagnostics and finite-size Lyapunov exponents computed from altimetry in the Algerian basin, *Deep Sea Res., Part I*, *56*(1), 15–31, doi:10.1016/j.dsr.2008.07.014.

Drijfhout, S. S., P. de Vries, K. Döös, and A. C. Coward (2003), Impact of eddy-induced transport on the Lagrangian structure of the upper branch of the thermohaline circulation, *J. Phys. Oceanogr.*, *33*(10), 2141–2155, doi:10.1175/1520-0485(2003)033 < 2141:IOE-TOT>2.0.CO;2.

Durrant, T. H., D. J. M. Greenslade, I. Simmonds, and F. Woodcock (2013), Correcting marine surface winds simulated in atmospheric models using spatially and temporally varying linear regression, *Weather Forecasting*, *29*(2), 305–330, doi:10.1175/WAF-D-12-00101.1.

Edwards, K. P., F. E. Werner, and B. O. Blanton (2006), Comparison of observed and modeled drifter trajectories in coastal regions: An improvement through adjustments for observed drifter slip and errors in wind fields, *J. Atmos. Oceanic Technol.*, *23*, 1614–1620, doi:10.1175/JTECH1933.1.

Ferrarin, C., and G. Umgiesser (2005), Hydrodynamic modeling of a coastal lagoon: The Cabras lagoon in Sardinia, Italy, *Ecol. Modell.*, *188*(2–4), 340–357, doi:10.1016/j.ecolmodel.2005.01.061.

Ferrarin, C., M. Bajo, D. Bellafiore, A. Cucco, F. De Pascalis, M. Ghezzo, and G. Umgiesser (2014), Toward homogenization of Mediterranean lagoons and their loss of hydrodiversity, *Geophys. Res. Lett.*, *41*, 5935–5941, doi:10.1002/2014GL060843.

Fischer, H. B., E. J. List, R. Y. C. Koh, J. Imberger, and N. H. Brooks (1979), *Mixing in Inland and Coastal Waters*, Academic, N. Y.

Foreman, M. G. G., L. Beauchemin, J. Y. Cherniawsky, M. A. Peña, P. F. Cummins, and G. Sutherland (2005), A review of models in support of oil and gas exploration off the north coast of British Columbia, *Can. Tech. Rep. Fish. Aquat. Sci. 2612*, Institute of Ocean Sciences Fisheries and Oceans Canada, 58 pp., Sidney.

Furnans, J., J. Imberger, and B. R. Hodges (2008), Including drag and inertia in drifter modelling, *Environ. Modell. Software*, *23*(6), 714–728, doi:10.1016/j.envsoft.2007.09.010.

Giorgi, F. (2006), Regional climate modeling: Status and perspectives, *J. Phys.*, *139*, 101–118.

Griffa, A., L. I. Piterbarg, and T. Özgökmen (2004), Predictability of Lagrangian particle trajectories: Effects of smoothing of the underlying Eulerian flow, *J. Mar. Res.*, *62*(1), 1–35.

Janjić, Z. I. (1984), Nonlinear advection schemes and energy cascade on semi-staggered grids, *Mon. Weather Rev.*, *112*(6), 1234–1245, doi:10.1175/1520-0493(1984)112 < 1234:NASAEC>2.0.CO;2.

Johnson, D., and C. Pattiaratchi (2004), Application, modelling and validation of surfzone drifters, *Coastal Eng.*, *51*(5–6), 455–471, doi:10.1016/j.coastaleng.2004.05.005.

Huntley, H. S., B. L. Lipphardt, and A. D. Kirwan (2011), Lagrangian predictability assessed in the East China Sea, *Ocean Modell.*, *36*(1–2), 163–178, doi:10.1016/j.ocemod.2010.11.001.

Kallos, G. (1997), The Regional weather forecasting system SKIRON, Proceedings, Symposium on Regional Weather Prediction on Parallel Computer Environments, 15–17 October 1997, 9 pp., University of Athens, Department of Physics, Department of Informatics, Athens, Greece.

Kallos, G., and I. Pytharoulis (2005), Short-term predictions (weather forecasting purposes, in *Encyclopedia of Hydrological Sciences*, edited by M. G. Anderson, pp. 2791–2811, John Wiley, London, U. K.

Koçak, M., C. Theodosi, P. Zarmpas, M. J. M. Séguret, B. Herut, G. Kallos, N. Mihalopoulosb, N. Kubilaya, and M. Nimmo (2012), Influence of mineral dust transport on the chemical composition and physical properties of the Eastern Mediterranean aerosol, *Atmos. Environ.*, *57*, 266–277, doi:10.1016/j.atmosenv.2012.04.006.

Kuzmić, M., I. Janeković, J. W. Book, P. J. Martin, and J. D. Doyle (2006), Modeling the northern Adriatic double-gyre response to intense bora wind: A revisit, *J. Geophys. Res.*, *112*, C03S13, doi:10.1029/2005JC003377.

Lebeaupin Brossier, C., K. Béranger, C. Deltel, and P. Drobinski (2011), The Mediterranean response to different space–time resolution atmospheric forcings using perpetual mode sensitivity simulations, *Ocean Modell.*, *36*(1–2), 1–25, doi:10.1016/j.ocemod.2010.10.008.

Lebeaupin Brossier, C., K. Béranger, and P. Drobinski (2012), Sensitivity of the northwestern Mediterranean Sea coastal and thermohaline circulations simulated by the 1/12°-resolution ocean model NEMO-MED12 to the spatial and temporal resolution of atmospheric forcing, *Ocean Modell.*, *43–44*, 94–107, doi:10.1016/j.ocemod.2011.12.007.

Lin, J. (2013), Lagrangian modeling of the atmosphere: An introduction, in *Lagrangian Modeling of the Atmosphere, Geophys. Monogr. Ser.*, vol. 200, pp. 225–233, AGU, Washington, D. C.
Lumpkin, R., and S. Elipot (2010), Surface drifter pair spreading in the North Atlantic, *J. Geophys. Res.*, *115*, C12017, doi:10.1029/2010JC006338.
Lynch, P. (2008), The origins of computer weather prediction and climate modeling, *J. Comput. Phys.*, *227*(7), 3431–3444.
Magni, P., S. Como, A. Cucco, G. De Falco, P. Domenici, M. Ghezzo, A. Perilli (2008), A multidisciplinary and ecosystemic approach in the Oristano Lagoon-Gulf system (Sardinia, Italy) as a tool in management plans, *Trans. Waters Bull.*, *2*(2), 41–62.
Manca, B. B., V. Kovačević, M. Gačić, and D. Viezzoli (2002), Dense water formation in the Southern Adriatic Sea and spreading into the Ionian Sea in the period 1997–1999, *J. Mar. Syst.*, *33–34*, 133–154, doi:10.1016/S0924-7963(02)00056-8.
Melaku Canu, D., C. Solidoro, V. Bandelj, G. Quattrocchi, R. Sorgente, A. Olita, L. Faziolic, and A. Cucco (2015), Assessment of oil slick hazard and risk at vulnerable coastal sites, *Mar. Pollut. Bull.*, *94*(1), 84–95, doi:10.1016/j.marpolbul.2015.03.006.
Millot, C. (1999), Circulation in the western Mediterranean Sea, *J. Mar. Syst.*, *20*(1–4), 423–442, doi:10.1016/S0924-7963(98)00078-5.
Molcard, A., P. M. Poulain, P. Forget, A. Griffa, Y. Barbin, J. Gaggelli, J. C. De Maistre, and M. Rixen (2009), Comparison between VHF radar observations and data from drifter clusters in the Gulf of La Spezia (Mediterranean Sea), *J. Mar. Syst.*, *78*, S79–S89, doi:10.1016/j.jmarsys.2009.01.012.
Monin A. S., and A. M. Obukhov (1954), Basic laws of turbulent mixing in the ground layer of the atmosphere, *Tr. Akad. Nauk SSSR Geophiz. Inst.*, *24*(151), 163–187.
Olita, A., A. Ribotti, L. Fazioli, A. Perilli, and R. Sorgente (2013), Surface circulation and upwelling in the Sardinia Sea: A numerical study, *Cont. Shelf Res.*, *71*, 95–108, doi:10.1016/j.csr.2013.10.011.
Olascoaga, M. J., I. I. Rypina, M. G. Brown, F. J. Beron-Vera, H. Koçak, L. E. Brand, G. R. Halliwell, and L. K. Shay (2006), Persistent transport barrier on the West Florida Shelf, *Geophys. Res. Lett.*, *33*, L22603, doi:10.1029/2006GL027800.
Ottimo, J. M. (1989), *The Kinematics of Mixing: Stretching, Chaos and Transport*, Cambridge Univ. Press, Cambridge, U. K.
Özgökmen, T. M., L. I. Piterbarg, A. J. Mariano, and E. H. Ryan (2001), Predictability of drifter trajectories in the tropical pacific ocean, *J. Phys. Oceanogr.*, *31*(9), 2691–2720, doi:10.1175/1520-0485(2001)031 < 2691:PODTIT>2.0.CO;2.
Papadopoulos, A., P. Katsafados, and G. Kallos (2001), Regional weather forecasting for marine application, *Global Atmos. Ocean Syst.*, *8*(2–3), 219–237.
Poulain, P.-M. (2001), Adriatic Sea surface circulation as derived from drifter data between 1990 and 1999, *J. Marine Systems*, *29*(1–4), 3–32, doi:10.1016/S0924-7963(01)00007-0.
Pullen, J., J. D. Doyle, R. Hodur, A. Ogston, J. W. Book, H. Perkins, and R. Signell (2003), Coupled ocean-atmosphere nested modeling of the Adriatic Sea during winter and spring 2001, *J. Geophys. Res.*, *108*(C10), 3320, doi:10.1029/2003JC001780.
Quattrocchi, G., A. Cucco, F. Antognarelli, A. Satta, F. Maicu, C. Ferrarin, and G. Umgiesser (2016), Optimal design of a Lagrangian observing system for hydrodynamic surveys, *J. Oper. Oceanogr.*, *9*, S77–S88, doi:10.1080/1755876X.2015.1114805.
Samelson, R. M., and S. Wiggins (2006), *Lagrangian Transport in Geophysical Jets and Waves: The Dynamical Systems Approach, Interdisciplinary Applied Mathematics*, vol. 31, Springer Science + Business Media, LLC, N. Y., doi:10.1007/978-0-387-46213-4.
Sammari, C., C. Millot, and L. Prieur (1995), Aspects of the seasonal and mesoscale variabilities of the Northern Current in the western Mediterranean Sea inferred from the PROLIG-2 and PROS-6 experiments, *Deep Sea Res., Part I*, *42*(6), 893–917, doi:10.1016/0967-0637(95)00031-Z.
Sayol, J. M., A. Orfila, G. Simarro, D. Conti, L. Renault, and A. Molcard (2014), A Lagrangian model for tracking surface spills and SaR operations in the ocean, *Environ. Modell. Software*, *52*, 74–82, doi:10.1016/j.envsoft.2013.10.013.
Serra, I. A., A. M. Innocenti, G. Di Maida, S. Calvo, M. Migliaccio, E. Zambianchi, C. Pizzigalli, S. Arnaud-Haond, C. M. Duarte, E. A. Serrao, and G. Procaccini (2010), Genetic structure in the Mediterranean seagrass *Posidonia oceanica*: Disentangling past vicariance events from contemporary patterns of gene flow, *Mol. Ecol.*, *19*(3), 557–568, doi:10.1111/j.1365-294X.2009.04462.x.
Signell, R. P., S. Carniel, L. Cavaleri, J. Chiggiato, J. D. Doyle, J. Pullen, and M. Sclavo (2005), Assessment of wind quality for oceanographic modelling in semi-enclosed basins, *J. Mar. Syst.*, *53*(1–4), 217–233, doi:10.1016/j.jmarsys.2004.03.006.
Simeone, S., G. De Falco, G. Quattrocchi, and A. Cucco (2014), Morphological changes of a Mediterranean beach over one year (San Giovanni Sinis, western Mediterranean), *J. Coastal Res.*, *70*, 217–222.
Smagorinsky, J. (1993), Some historical remarks on the use of non-linear viscosities, in *Large Eddy Simulation of Complex Engineering and Geophysical Flows*, edited by B. Galperin and S. A. Orszag, pp. 3–36, Cambridge Univ. Press, Cambridge, U. K.
Speich, S., B. Blanke, P. de Vries, S. Drijfhout, K. Döös, A. Ganachaud, and R. Marsh (2002), Tasman leakage: A new route in the global ocean conveyor belt, *Geophys. Res. Lett.*, *29*(10), 1416, doi:10.1029/2001GL014586.
Spydell, M. S., F. Feddersen, M. Olabarrieta, J. Chen, R. T. Guza, B. Raubenheimer, and S. Elgar (2015), Observed and modeled drifters at a tidal inlet, *J. Geophys. Res. Oceans*, *120*, 4825–4844, doi:10.1002/2014JC010541.
Stark, J. D., C. J. Donlon, M. J. Martin, and M. E. McCulloch (2007), OSTIA: An operational, high resolution, real time, global sea surface temperature analysis system, in *Oceans*, pp. 1–4, IEEE, Aberdeen, Scotland.
Taylor, K. E. (2001), Summarizing multiple aspects of model performance in a single diagram, *J. Geophys. Res.*, *106*(D7), 7183–7192, doi:10.1029/2000JD900719.
Thompson, K. R. (2003), Prediction of surface currents and drifter trajectories on the inner Scotian Shelf, *J. Geophys. Res.*, *108*(C9), 3287, doi:10.1029/2001JC001119.
Ullman, D. S., J. O'Donnell, J. Kohut, T. Fake, and A. Allen (2006), Trajectory prediction using HF radar surface currents: Monte Carlo simulations of prediction uncertainties, *J. Geophys. Res.*, *111*, C12005, doi:10.1029/2006JC003715.
Umgiesser, G., D. M. Canu, A. Cucco, and C. Solidoro (2004), A finite element model for the Venice Lagoon. Development, set up, calibration and validation, *J. Mar. Syst.*, *51*(1–4), 123–145, doi:10.1016/j.jmarsys.2004.05.009.
Umgiesser, G., C. Ferrarin, A. Cucco, F. De Pascalis, D. Bellafiore, M. Ghezzo, and M. Bajo (2014), Comparative hydrodynamics of 10 Mediterranean lagoons by means of numerical modeling, *J. Geophys. Res. Oceans*, *119*, 2212–2226, doi:10.1002/2013JC009512.
van Sebille, E., P. J. van Leeuwen, A. Biastoch, C. N. Barron, and W. P. M. de Ruijter (2009), Lagrangian validation of numerical drifter trajectories using drifting buoys: Application to the Agulhas system, *Ocean Modell.*, *29*(4), 269–276, doi:10.1016/j.ocemod.2009.05.005.
Wang, J., and Y. Shen (2010), Modeling oil spills transportation in seas based on unstructured grid, finite-volume, wave-ocean model, *Ocean Modell.*, *35*(4), 332–344, doi:10.1016/j.ocemod.2010.09.005.
Wakelin, S. L., and R. Proctor (2002), The impact of meteorology on modelling storm surges in the Adriatic Sea, *Global Planet. Change*, *34*(1–2), 97–119, doi:10.1016/S0921-8181(02)00108-X.
Yaremchuk, M., P. Spence, M. Wei, and G. Jacobs (2013), Lagrangian predictability in the DWH region from HF radar observations and model output, *Deep Sea Res., Part II*, *129*, 394–400, doi:10.1016/j.dsr2.2013.05.035.

Zavatarelli, M. (2002), Diagnostic and prognostic model studies of the Adriatic Sea general circulation: Seasonal variability, *J. Geophys. Res.*, *107*(C1), 3004, doi:10.1029/2000JC000210.

Zecchetto, A., F. De Biasio, A. della Valle, A. Quattrocchi, E. Cadau, and A. Cucco (2016), Wind Fields From C- and X-Band SAR Images at VV Polarization in Coastal Area (Gulf of Oristano, Italy), *IEEE J. Sel. Top. in App. Earth Obs. and Remote Sen*., *99*, 1–8, doi:10.1109/JSTARS.2016.2538322.

Zecchetto, A., A. della Valle, F. De Biasio, G. Quattrocchi, G. A. Satta, F. Antognarelli, E. Cadau, and A. Cucco (2016a), The wind measuring system in the Gulf of Oristano: A support to coastal scale oceanographic applications, *J. Oper. Oceanogr*., *9*, s144–s154, doi:10.1080/1755876x.2015.1118806.

Zecchetto, S., and C. Accadia (2014), Diagnostics of T1279 ECMWF analysis winds in the Mediterranean basin by comparison with ASCAT 12.5 km winds, *Q. J. R. Meteorol. Soc*., *140*(685), 2506–2514, doi:10.1002/qj.2315.

Zecchetto, S., G. Umgiesser, and M. Brocchini (1997), Hindcast of a storm surge induced by local real wind fields in the Venice Lagoon, *Cont. Shelf Res*., *17*(12), 1513–1538, doi:10.1016/S0278-4343(97)00023-X.